



Enhancement of Antioxidative and Anti-Inflammatory Activities of Corn Silk Polysaccharides After Selenium Modification

Yu-Yun Zheng, Xin-Yi Tong , Da-Ying Zhang, Jian-Ming Ouyang 

Institute of Biomineralization and Lithiasis Research, College of Chemistry and Materials Science; Jinan University, Guangzhou, 510632, People's Republic of China

Correspondence: Jian-Ming Ouyang, Email toymj@jnu.edu.cn

Objective: This study aimed to study the effect of selenium modification on the bioactivity of corn silk polysaccharides, particularly its antioxidant and anti-inflammatory functions.

Methods: $\text{HNO}_3\text{-NaSeO}_3$ was used to selenize degraded corn silk polysaccharides (DCSP). The structure and physicochemical properties of DCSP and selenized corn silk polysaccharides (Se-DCSP) were characterized by inductively coupled plasma emission spectroscopy, Fourier-transform infrared, ultraviolet–visible spectroscopy, nuclear magnetic resonance, nanometer, scanning electron microscopy, and thermogravimetric analysis. The protective effects of DCSP and Se-DCSP on HK-2 cells damaged by nano-calcium oxalate and the changes of inflammatory factors were detected by laser confocal microscopy, flow cytometry, and fluorescence microscopy.

Results: The selenium content of DCSP and Se-DCSP were 19.5 and 1226.7 $\mu\text{g/g}$, respectively. Compared with DCSP, Se-DCSP showed significantly improved biological activity, including the scavenging ability of various free radicals (increased by about 2–3 times), the intracellular reactive oxygen content (decreased by about 1.5 times), and the mitochondrial membrane potential (decreased by about 2.5 times). Moreover, cell viability and morphological recovery ability were improved. Compared with DCSP, Se-DCSP significantly down-regulated HK-2 cell inflammatory factors MCP-1 (about 1.7 times), NLRP3, and NO (about 1.5 times).

Conclusion: The antioxidant activity and the ability to down-regulate the expression of inflammatory factors of Se-DCSP were significantly enhanced compared with DCSP, and Se-DCSP can better protect HK-2 cells from oxidative damage, indicating that Se-DCSP has a stronger potential ability to inhibit kidney stone formation.

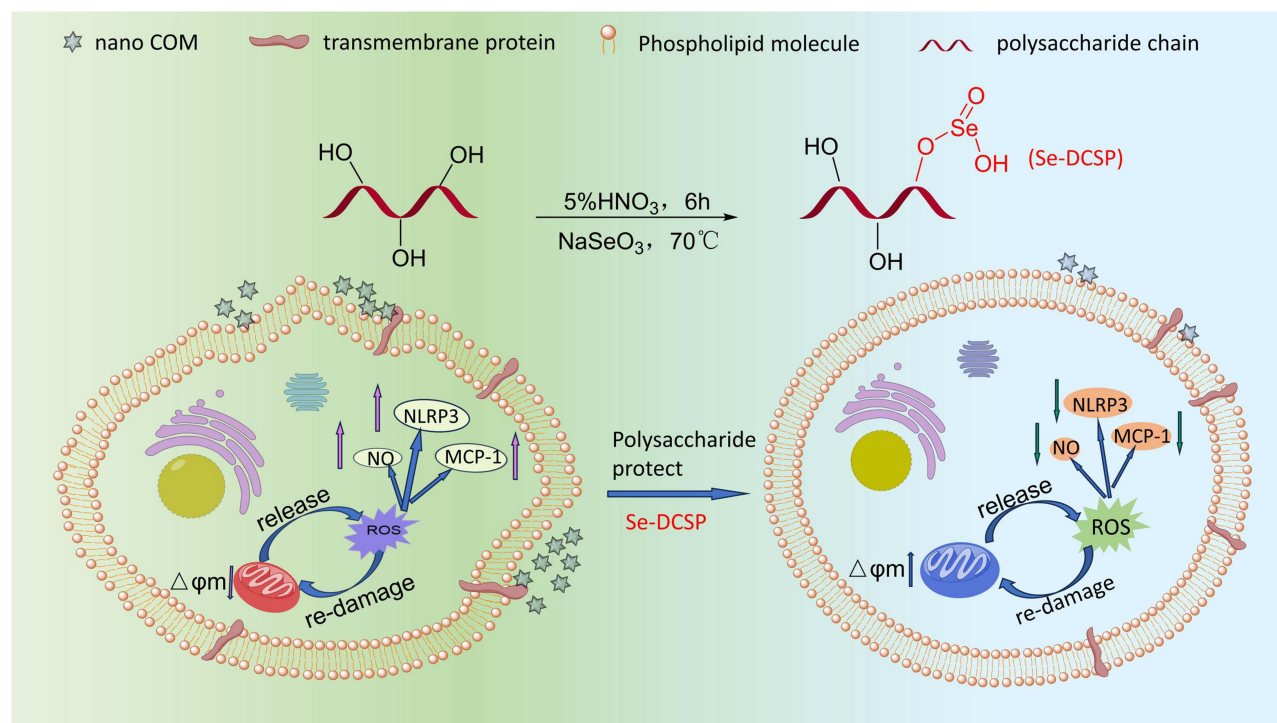
Keywords: selenization, corn silk polysaccharide, antioxidant, cell protection, inflammation

Introduction

Kidney stone is a common urinary system disease with high incidence.¹ Kidney stone is composed of calcium oxalate (65.9%), carbon apatite (15.6%), uric acid (UA) salt (12.4%), magnesium ammonium phosphate (struvite, 2.7%), and permeate phosphorite (1.7%).² The formation of kidney stones is closely related to the degree of damage of renal epithelial cells. Damaged cells can cause reactive oxygen species (ROS) production, which leads to oxidative stress and mitochondrial dysfunction, as well as induces the overexpression of adhesion molecules such as osteopontin and CD44 on the cell surface, making it easier for crystals to adhere to the cell surface and increasing the risk of kidney stone formation.³ After protecting the cells or repairing the damaged cells, oxidative stress can be reduced, and the formation of kidney stones can be effectively inhibited.

Selenium is a trace element essential for human health. However, selenium cannot be synthesized in organisms and can be obtained from food and supplements.⁴ The kidney has the highest selenium content of all organs and has the ability to synthesize different selenoproteins.⁵ Related studies have shown that selenium is an essential trace element to maintain kidney structure and function. Chronic kidney disease and end-stage renal disease are usually associated with

Graphical Abstract



low selenium levels in serum and tissues, and selenium deficiency can damage the ultrastructure and extracellular matrix of glomeruli and tubules.⁶ Wang et al⁷ reported that Se could inhibit the mitochondrial apoptosis pathway in renal dysfunction mediated by oxidative stress caused by heavy metals by activating c-jun N-terminal kinase (JNK) phosphorylation and blocking ROS production. In this paper, selenium and corn silk polysaccharide are organically combined in order to develop anti-calculus polysaccharides with stronger activity.

The biological activity of polysaccharides is closely related to its structure. Changing the chemical structure of polysaccharides or introducing functional groups (such as hydroxyl, amino, carboxyl, and sulfate groups) can enhance the existing biological activities of polysaccharides or produce new biological activities.⁸ Among them, the carboxymethylation, sulfation, phosphorylation, and selenation of polysaccharides have been widely reported.⁹

Natural Se polysaccharides are usually found in plants or microorganisms, but even plants grown in high-Se areas have low Se content. If inorganic selenium and polysaccharide could be combined to form organic selenium polysaccharides, then the biological activities of polysaccharide and selenium can be exerted simultaneously.¹⁰

Hamid et al¹¹ found that astragalus selenide polysaccharide could downregulate the expression of inflammatory factors IL-6 and TNF- α , improve CCl₄-induced liver injury in rats by inhibiting inflammatory response, and prevent liver injury and fibrosis. Huang et al¹² reported that astragalus selenide polysaccharide could effectively protect renal epithelial cell damage caused by nanoCOM, reduce crystal adhesion on the cell surface, and enhance the antioxidant activity of polysaccharides. Liu et al¹³ showed that organic selenium yeast could effectively inhibit the formation of calcium oxalate stones induced by ethylene glycol in dogs by improving the antioxidant capacity in vivo. Therefore, the study of organic selenium drugs is of great significance for the treatment of kidney stones. However, the application of selenopolysaccharides in the prevention and treatment of kidney stones is rarely reported.

Corn silk contains a variety of bioactive components that have significant effects on human health, such as polysaccharides, flavonoids, and alkaloids. The biological activities of corn silk include antioxidant activity,¹⁴ anti-diabetic activity,¹⁵ anticoagulant activity,¹⁶ and anti-inflammatory activity.¹⁷

Wang et al¹⁸ extracted and purified neutral corn silk polysaccharide (NCSP) and acidic corn silk polysaccharide (ACSP). Experiments have shown that NCSP and ACSP could target the kidney and possess therapeutic effects on renal excretion dysfunction. These characteristics of NCSP and ACSP are due to their ability to inhibit serum UA secretion and xanthine oxidase activity, thereby reducing glomerular and renal tubule damage in vivo. Zou et al¹⁹ proved that carboxylated CSP could significantly improve its antioxidant capacity, regulate calcium oxalate monohydrate to calcium oxalate dihydrate, which has less damage to HK-2 cells, reduce the adhesion of crystals on the cell surface, and inhibit stone formation.

Based on the abovementioned contents and related technologies, in this study, the degraded corn silk polysaccharide (DCSP) was selenized, and the protective effect of CSP on HK-2 cells against oxidative damage before and after selenization was investigated. From the perspective of reducing oxidative stress and anti-inflammation, the potential ability of CSP to reduce the risk of kidney stone formation was discussed, which can provide an alternative for the development of green anti-stone drugs.

Experimental Methods

Materials and Apparatus

Material

Corn silk protopolysaccharide (CSP) was produced by Qingzhi Biological Co., LTD. Human renal proximal tubular epithelial cells (HK-2) were purchased from the Shanghai Cell Bank of the Chinese Academy of Sciences (Shanghai, China). Fetal bovine serum and cell culture medium (DMEM-F12) were purchased from Haichun Biochemical Products (Beijing) Co., LTD. (Beijing, China). DAPI was obtained from KeyGEN Biotechnology Co. (Nanjing, China). Cell proliferation assay kit (CCK-8) and reactive oxygen species detection kit (DCFH-DA) were purchased from Shanghai Beyotime Biotechnology Co., LTD. PBS, phenoazine, 1, 1-diphenyl-2-trinitrophenylhydrazine (DPPH), phenanthrene and other conventional reagents were all pure analytical reagents, provided by Guangzhou Chemical Reagents Co., LTD.

Apparatus

Fourier transform infrared absorption spectrometer (USA). Nuclear magnetic resonance instrument (Varian Bruker-500 MHz). Ultrasonic instrument (allied JP-100S). Ullmann viscometer (capillary inner diameter 0.45 mm). Thermogravimetric analyzer (TGA/DSC3⁺, Mettler Toledo, USA). D/ MAX2400 X-ray powder diffractometer (Japan). Field emission scanning electron microscope (ULTRA55, Zeiss, Germany). OPTIMA-2000DV inductively coupled Plasma Emission Spectrometer (ICP) (PE Company, USA). Inverted fluorescence microscope (IX51, OLYMPUS, Japan). Flow cytometry (FACS Aria, BD, USA). Microplate reader (SafireZ, Tecan, Switzerland).

Selenized Corn Silk Polysaccharide

Degradation of Corn Silk Polysaccharide

1.20 g of original corn silk polysaccharide (CSP) was accurately weighed and dissolved in 20 mL distilled water at 70°C. When the temperature reaches 90°C, 5 mL of 30% hydrogen peroxide was quickly added to make the concentration of hydrogen peroxide in the degradation system to 6%. The polysaccharide was degraded at 90°C for 2 h, cooled to room temperature, and the pH was adjusted to 7.0 with 2 mol/L NaOH solution. Then the polysaccharide solution was concentrated to 1/3 of its original volume under reduced pressure at 60°C, then precipitated by 3 times the volume of anhydrous ethanol, placed overnight, centrifuged, and dried to obtain degraded polysaccharide (DCSP).

Selenization of DCSP

The experimental procedure was slightly improved by referring to the reference.²⁰ DCSP (1 g) was dissolved in 50 mL 5% HNO₃, heated and stirred in a water bath at 70°C, then 600 mg Na₂SeO₃ and 1.0 g BaCl₂ were added, and reacted for 6 h. The pH value of the solution was adjusted to 7–8 with 1 mol/L NaOH. Excessive Na₂SO₄ was added to remove Ba²⁺ ions from the solution. Centrifuge and collect the supernatant. The supernatant was dialysed until Na₂SeO₃ was completely removed. The specific process is: take out a small amount of dialysate every 6 h, add ascorbic acid until

there is no red color, which indicates that the free Na_2SeO_3 in the solution is completely removed. Stop dialysis. The solution after dialysis was concentrated, precipitated with anhydrous ethanol and dried to obtain Se-DCSP.

Determination of Selenium Content in Se-DCSP

Dissolve 20 mg Se-DCSP in 5 mL mixed acid ($\text{HCl}:\text{HNO}_3=3:1$), cold digestion at 4°C for 24 h, and then heating at 180°C until the solution is clear, colorless and accompanied by white smoke (during which concentrated HNO_3 is constantly added), continue heating and concentration to 2 mL. The concentrated liquid was cooled and filtered, and set to 10 mL with distilled water. The selenium content was detected by ICP.

X-Ray Photoelectron Spectroscopy (XPS) Analysis

XPS testing of polysaccharides before and after selenization was performed using a K-Alpha+ spectrometer from Thermo Fisher Scientific. The samples were first dried under vacuum, the X-ray source was set to Al K α , the energy was set to 1486.6 eV, 6 mA \times 12 KV, and the binding energy was corrected by C1s ($\text{BE} = 284.8 \text{ eV}$).

Structural Characterization of Se-DCSP and DCSP

Determination of Molecular Weight of Polysaccharides

According to literature,²¹ the viscosity of polysaccharide solution was measured by Ullmann viscosity method at $25 \pm 0.2^\circ\text{C}$. After measuring the falling time (T) of each polysaccharide in the viscometer, the relative viscosity η_r and the increasing viscosity η_{sp} were calculated, where $\eta_r = T_i/T_0$, $\eta_{sp} = \eta_r - 1$, where T_i and T_0 are the falling time of the polysaccharide solution and deionized water, respectively. The characteristic viscosity $[\eta] = [2(\eta_{sp} - \ln \eta_r)]^{1/2}/c$ was obtained by the one-point formula, where c is the concentration of the sample to be measured. The molecular weight of each polysaccharide before and after degradation was calculated from the $[\eta]$ value. Because the relationship between the intrinsic viscosity of the polymer solution $[\eta]$ and the molecular weight (M) of the polymer can be expressed by the Mark-Houwink empirical equation: $[\eta] = \kappa M^\alpha$, where κ and α are the two parameters of the empirical equation, they are constants related to the polymer morphology, solvent and temperature.

Scanning Electron Microscope (SEM) Observation

Morphological characteristics of DCSP and Se-DCSP were observed by SEM. The sample is fixed to the sample holder with carbon tape and then sputtered with gold powder using an ion sputtering coater. The sample was observed at 3 kV acceleration voltage.

TGA Analysis

The thermogravimetric analysis curve of corn silk polysaccharide before and after selenization was determined and its thermal stability was analyzed. The experimental process was referred to literature²² and slightly improved. The experimental conditions were as follows: the heating rate of nitrogen stream was $10^\circ\text{C}/\text{min}$, and the temperature was $25\text{--}900^\circ\text{C}$.

FT-IR and UV-Visible Spectra

Take a 2.0 mg dry DCSP or Se-DCSP sample, mix the sample with 200 mg KBr, and grind the mixture until there are no visible particles. Subsequently, the powder was pressed into a disc by a press. After background interference was eliminated, appropriate experimental parameters were set, and sample scanning was performed.

Polysaccharides (DCSP and Se-DCSP) were dissolved and diluted to appropriate concentration. These samples were scanned from 200 to 600 nm by an ultraviolet spectrophotometer.

XRD Analysis

The XRD patterns of DCSP and Se-DCSP were determined with a D/max2400 X-ray powder diffractometer (Nippon Nippon Science). Data were collected with a 2θ range of 5 to 70° , a tube pressure of 40 kV, a tube flow of 25 mA, and a scan rate of $8^\circ/\text{min}$.

Zeta Potential

DCSP or Se-DCSP was dissolved in deionized water to prepare 0.20 mg/mL polysaccharide solution. The Zeta potential of the polysaccharide was detected by a nanometer particle size meter.

Monosaccharide Composition

The monosaccharide components of DCSP were analyzed and detected by ion chromatography system (ICS 5000+, Thermo Fisher Scientific, USA) with electrochemical detector.

ID and 2D NMR Detection of Polysaccharides

The 35 mg completely dried polysaccharide sample was weighed and added to NMR tube containing 0.5 mL of deuterated water (D₂O). Note that this operation should be carried out in a fume hood, and repeated blowing with a pipet gun until completely dissolved to avoid bubbles, and further transferred to a nuclear magnetic tube until detection.

Antioxidant Activity

Ability to Scavenge Hydroxyl Radicals

H₂O₂/Fe system method was used to test the ability of removing •OH in vitro before and after selenization.²³ FeSO₄ solution (2.5 mmol/L, 1 mL) and o-phenylene solution (2.5 mmol/L, 1 mL) were added to the test tube, respectively. Phosphoric acid buffer (PBS) (20 mmol/L, 1 mL) and H₂O₂ (20 mmol/L, 1 mL) were added successively at a pH of 7.4, and finally 1 mL polysaccharide solution was added (the final concentration was 0.25, 0.50, 1.00, 2.00, 3.00 mg/mL, respectively). After the mixture was evenly mixed, it was kept at 37°C for 90 min, and the absorbance was detected by ultraviolet spectrophotometer at 536 nm, which was repeated twice to obtain the average absorbance (A3). In the undamaged group, the volume was filled with distilled water without adding sugar solution and hydrogen peroxide, and the absorbance was A2. The damaged group was filled with distilled water without adding polysaccharide solution, and the absorbance was A1. Ascorbic acid (Vc) was used as positive control group.

$$\text{OH clearance \%} = \frac{A3 - A1}{A2 - A1} \times 100 \quad (1)$$

Ability to Scavenge DPPH Free Radicals

The experiment was slightly improved on the basis of the literature.²³ DPPH was prepared into 0.4 mmol/L DPPH solution with anhydrous ethanol. 3 mL polysaccharide solution (final concentration of 0.25, 0.50, 1.00, 2.00 and 3.00 g/L) and 0.4 mmol/L DPPH solution 1 mL were mixed in a test tube. The final concentration of DPPH was 0.1 mmol/L, and the absorbance was measured at 517 nm after 30 min in a dark room at 25°C, with Vc as the positive control.

$$\text{DPPH clearance \%} = 1 - \frac{(A2 - A1)}{A0} \times 100 \quad (2)$$

A0 was the absorbance value of 1 mL DPPH solution mixed with 3 mL distilled water. A1 was the absorbance value of mixing 3 mL sample solution with 1 mL blank solvent (anhydrous ethanol). A2 was the absorbance value of 3 mL sample solution mixed with 1 mL DPPH reagent.

ABTS Free Radical Scavenging

The experiment was based on reference²⁴ with some modifications. 7 mmol/L ABTS reagent was mixed with 2.45 mmol/L potassium persulfate reagent at a volume ratio of 1:1, and the reaction was placed in the dark for 12–16 h at room temperature. Then, 3 mL test solution and 1 mL polysaccharide solution of each concentration (final concentration 0.25–3 mg/mL) were mixed in a test tube, reacted at 25°C for 6 min, and the absorbance was determined at 734 nm.

$$\text{ABTS clearance \%} = 1 - \frac{(A1 - A2)}{A0} \times 100 \quad (3)$$

A0 was the control group (without polysaccharide). A1 is the experimental group; A2 is the background group (without reagents).

Cell Culture and Cell Treatment

Cell Viability Detected by CCK-8

The cell toxicity test of polysaccharides was divided into the following groups: (A) blank background group; (B) Polysaccharide protection group with polysaccharide concentration of 30–120 µg/mL.

Cell survival test under polysaccharide protection was divided into 3 groups: 1) control group: serum free medium only; 2) Damage group: 200 µg/mL nanoCOM in serum free medium; 3) DCSP/Se-DCSP protected group: DCSP or Se-DCSP with concentrations of 30, 60, 90 and 120 µg/mL, and 200 µg/mL nanoCOM crystals in serum free medium.

The Cells were implanted in 96-well culture plates at a density of 1.0×10^5 Cells /mL and treated until the fusion was about 80%. After incubation, 10 µL of CCK-8 reagent was added. The cells were incubated away from light for 1–4 h. The absorbance was detected at 450 nm using a microplate reader.

Cell Morphology Detected by HE Staining

Cells were seeded in 6-well culture plates at a concentration of 1×10^5 cells/mL in 1 mL/well. Cell morphology test was divided into 3 groups: (A) blank control group: serum free medium only; (B) damage group: 200 µg/mL nanoCOM in serum free medium; (C) protected group: 60 µg/mL polysaccharide and 200 µg/mL nanoCOM mixture (pre-mixed for 15 minutes) were added. After incubation for 24 h, the cells in each group were fixed with 4% paraformaldehyde for 15 min. Then, the cells were stained with hematoxylin and eosin staining solution for 15 min and 5 min, respectively. The unbound dyes were washed away. The morphology of the cells was observed under a microscope.

DCFH-DA Staining Confocal Detection ROS

The experimental groups were the same as 2.5.2 “Cell Morphology Detected by HE Staining”. Cells in each group were incubated for 24 h, and DCFH-DA was diluted in serum-free medium at a rate of 1:1000 to a final concentration of 10 µmol/L. The cell culture medium was removed and 1 mL of diluted DCFH-DA was added. The cells were incubated in a cell incubator at 37°C for 20 min. The cells were washed three times with serum-free cell culture medium to adequately remove extracellular residual DCFH-DA. The fluorescence intensity of ROS was observed by confocal microscopy.

Detection the Mitochondrial Membrane Potential

The grouping of cells was the same as in 2.5.2 “Cell Morphology Detected by HE Staining”. After 24 h of incubation, the supernatant was discarded and washed twice with PBS. JC-1 dye was diluted in serum-free medium at 1:1000. 1 mL of diluted JC-1 was added and incubated in a cell incubator at 37°C for 30 min, then the supernatant was discarded and washed three times with PBS to fully remove JC-1 that did not enter the cells.

After JC-1 cells were stained, the fluorescence intensity of mitochondrial membrane potential was directly observed by laser confocal microscope. Or pancreatic enzymes collect cells after digestion. Cells were resuspended in PBS for detection by flow cytometry.

Polysaccharide Anti-Inflammatory Test

Confocal Laser Scanning Microscope Observation of MCP-1 Expression

Cells were grouped as in 2.5.2 “Cell Morphology Detected by HE Staining”. After incubation for 24 h, the supernatant was discarded, washed twice with PBS, fixed with 4% paraformaldehyde for 15 min, treated with immunostaining permeabilization buffer with Triton X-100 for 10 min, washed twice with immunostaining wash solution, and treated with blocking solution (BSA) for 20 min. The cells were incubated with primary MCP-1 antibody at 4°C overnight. The primary antibody was recovered and the green fluorescent sheep anti-mouse secondary antibody was added, incubated at room temperature for 2 h, washed twice with immunostaining wash solution, incubated with DAPI for 10 min, washed twice with immunostaining wash solution. Finally, laser confocal scanning microscope was used for observation.

NLRP3 Immunofluorescence Detection

Cell culture and grouping were the same as in 2.5.2 “Cell Morphology Detected by HE Staining”. NLRP3 primary antibody was added and incubated overnight at 4°C. Other procedures were the same as 2.6.1 “Confocal Laser Scanning Microscope Observation of MCP-1 Expression”.

Nitric Oxide (NO) Content Detection

Cell culture and grouping were the same as in 2.5.2 “Cell Morphology Detected by HE Staining”. DAF-FM DA was diluted with appropriate fresh medium (free of serum and phenol red) at a ratio of 1:1000 to a final concentration of 5 $\mu\text{mol/L}$. At the end of the incubation, the cell culture medium was discarded and the appropriate volume of diluted DAF-FM DA was added. After 20 minutes of incubation in the cell incubator at 37°C, the cells were washed three times with PBS to fully remove the extracellular residual DAF-FM DA, and observed under fluorescence microscope.

Statistical Analysis

The experimental results were statistically analyzed using SPSS 26.0 software (SPSS Inc., Chicago, IL, USA), and the Tukey’s test was used to analyze the differences between the means of each experimental group and the control group. P values less than 0.05 were considered statistically significant.

Results

Preparation and Characterization of the Physicochemical Properties of DCSP and Se-DCSP

Changes in the Degradation and Properties of CSPs

The original CSP with a Mw of 31.8 kDa was degraded by 6% H_2O_2 . The resulting degraded polysaccharide (DCSP) had a Mw of 15.8 kDa and a reduced viscosity (from 5.54 to 2.75 mL/g).

Detection of Selenium Content in DCSP

The degree of CSP selenization was greatly affected by the reaction temperature and nitric acid concentration. When the temperature was below 60 °C or the final concentration of nitric acid was below 3.75%, selenization could not be successful. The reaction time and amount of catalyst had relatively little effect on selenization. However, the yield of selenification was low under all conditions.

When CSP was degraded, the degree of selenization of the degraded polysaccharide (DCSP) was significantly increased (Table 1). The optimal selenization conditions for DCSP were as follows: temperature of 70 °C, reaction time of 6 h, and final nitric acid concentration of 5%. The results of ICP-AES showed that the selenium content in Se-DCSP was 1227 $\mu\text{g/g}$, which was significantly higher than that in DCSP before selenification (19.5 $\mu\text{g/g}$).

XPS Analysis

XPS spectra of DCSP and Se-DCSP are shown in Figure 1. Compared with DCSP, Se-DCSP has two new peaks at 165.88 and 60.73 eV, corresponding to the Se 3p_{3/2} peak and Se 3d peak, respectively, indicating that the selenium group is a form of selenite.²⁵ In addition, the O1s binding energy of DCSP is 534.44 eV, whereas that of Se-DCSP is 532.81 eV, which is attributed to the substitution of selenite for some H atoms in the OH group during selenization, resulting in a decrease in the electron density around O atoms²⁶ and a weakening of the internal electron shielding effect. The electron binding energy of O1s increases. Figure 1E and F show the C 1s spectrum and curve fitting of DCSP and Se-DCSP, respectively. The C 1s spectrum of DCSP consists of three binding energy peaks centered at 284.80, 287.16, and 288.85 eV, which are attributed to C-O, C-OH, and C=O, respectively.²⁷ For Se-DCSP, the O/C ratio of 2.11 (66.64/

Table 1 Synthesis Conditions and Selenium Content of Selenized DCSP

Sample	Mw/ kDa	[η] mL/g	Reaction Time / h	NaSeO ₃ Dosage / mg	Temperature Reflex / °C	HNO ₃ (v/v)	Selenium Content / $\mu\text{g/g}$
CSP	31.8 \pm 1.4	5.54	0	–	–	–	22.0
DCSP	15.8 \pm 0.4	2.75	0	0	–	–	19.5
Se-DCSP	12.0 \pm 0.9	2.09	6	600	70	5%	1227

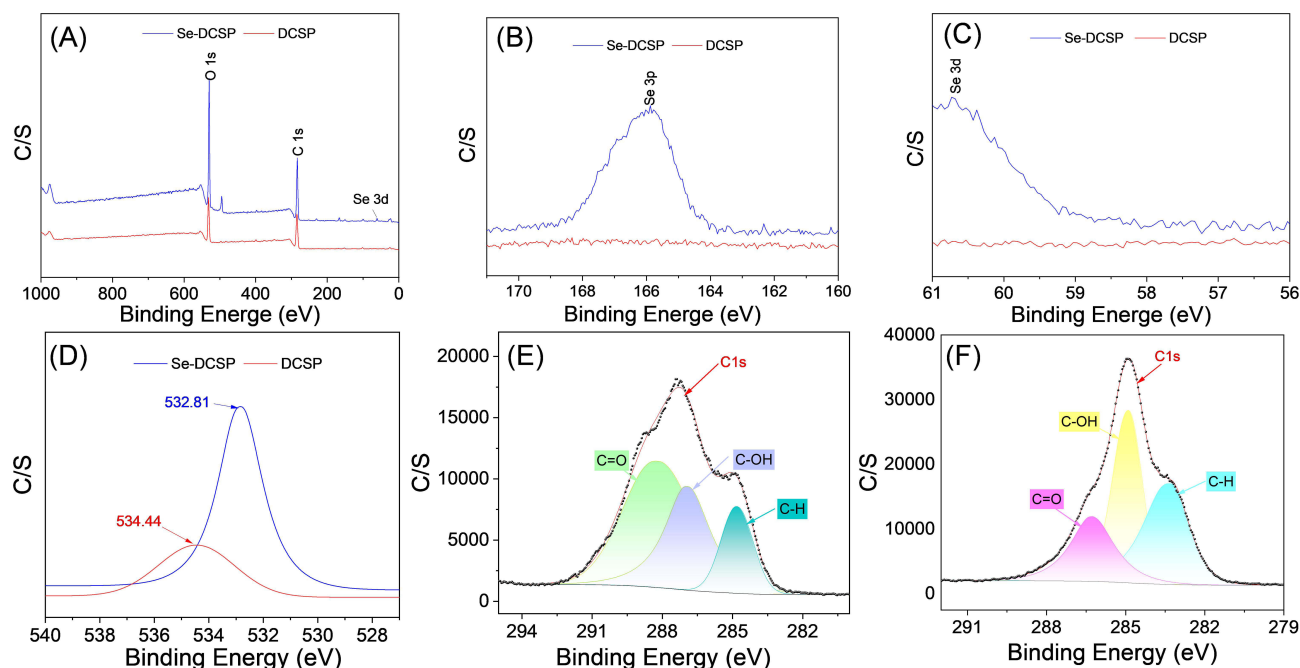


Figure 1 XPS spectra analysis of DCSP and Se-DCSP. (A) Survey spectra; (B) Se-3p spectra; (C) Se-3d spectra; (D) O 1s spectra; (E) C 1s curve-fitting of DCSP; (F) C 1s curve-fitting of Se-DCSP.

31.57) was obtained, which was higher than that of 1.23 (50.68/41.16) for DCSP. The increase of the O/C ratio indicates that the oxygen content after modification is higher than that before modification.²⁵ Furthermore, Se has been successfully introduced into DCSP, and this element exists as a selenate group (SeO_3^{2-}).

Molecular Weight of Polysaccharides

The Mw of each polysaccharide was determined by using an Ullmann viscometer. The Mw of DCSP was 15.8 kDa, which was lower than that of CSP before degradation (31.7 kDa, Table 1). After selenization of DCSP, the Mw of Se-DCSP was 12.0 kDa, which was lower than that of DCSP before selenization. The reduction of Mw is due to the selenization of polysaccharides, which was carried out in strong acid at 70 °C, at which time part of the sugar chain is broken, leading to the reduction of Mw.⁶ Zhao et al²⁸ also found that the Mw of PRSP-1, PRSP-2, and PRSP-3 (whose selenium contents were $170 \pm 12 \mu\text{g/g}$, $320 \pm 10 \mu\text{g/g}$, and $480 \pm 8 \mu\text{g/g}$, respectively) decreased by 24.23%, 36.98%, and 55.51%, respectively, compared with those before selenization.

Morphology of Polysaccharides Observed by SEM

The microscopic surfaces of DCSP and Se-DCSP were observed by SEM (Figure 2). Before selenification, DCSP was bulk and porous. However, the selenized DCSP became spherical and granular, with a significant reduction in size and a uniform distribution, which increased its solubility and biological activity.

TGA Analysis

The TGA curve of DCSP (Figure 3A) shows the weight loss of three stages (I, III, IV), whereas the TGA curve of Se-DCSP (Figure 3B) presents four weight loss stages (I, II, III, IV).

Stage I was the loss of free water. DCSP occurred between 30.98 °C and 114.57 °C, with a mass loss of 5.14%, and the maximum decomposition rate was 65.83 °C. Se-DCSP occurred at 26.06 °C–119.78 °C with a weight loss of 4.77% and a maximum decomposition rate of 70.67 °C.

Stage III was the decomposition of polysaccharides, in which the DCSP occurred at 114.57 °C–547.27 °C with a weight loss of 48.88%, and the maximum decomposition rate was 304.51 °C. Se-DCSP occurred at 178.17 °C–568.52 °C with a weight loss of 58.39% and a maximum decomposition rate of 309.33 °C. This process started with

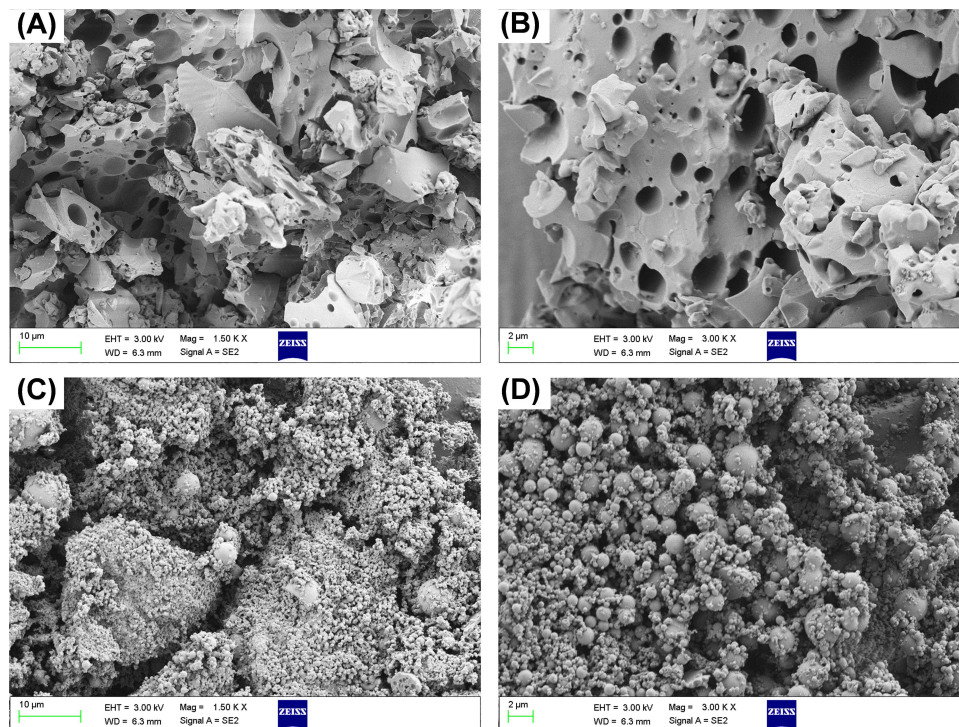


Figure 2 SEM observation of DCSP and Se-DCSP. (A and B) DCSP; (C and D) Se-DCSP. Scale bar: (A and C) 10 μ m; (B and D) 2 μ m.

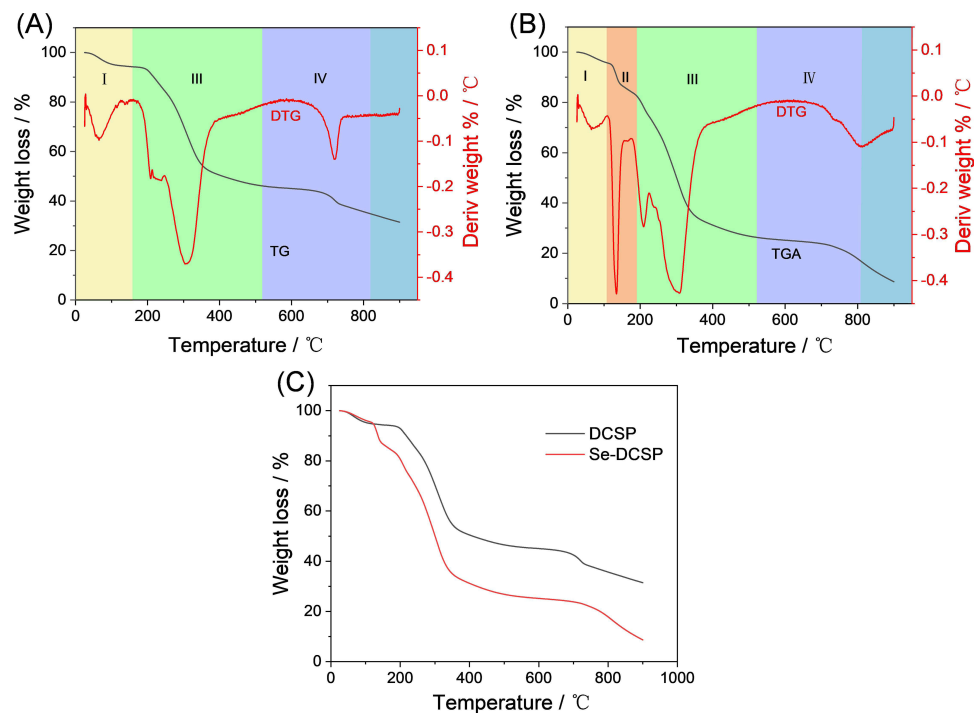


Figure 3 TGA and DTG curves of DCSP and Se-DCSP. (A) DCSP; (B) Se-DCSP; (C) TGA comparison chart of DCSP and Se-DCSP.

a drastic thermal degradation of the side chain of the polysaccharide, followed by the decarboxylation of the carbon in the acid side group and the ring, and finally the release of different gaseous products and different forms of solid carbon.²⁹

Stage IV was the further oxidation of organic matter, in which DCSP occurred at 547.27 °C–889.56 °C with a weight loss of 14.11%. Se-DCSP occurred at 547.27 °C–889.56 °C with a weight loss of 14.11%. Corazzari et al³⁰ reported the generation of CH₄ gas, resulting in mass reduction.

The decomposition temperatures and products of the above three processes DCSP and Se-DCSP are similar.

Stage II was slightly special. At stage II, the weight loss of Se-DCSP was 11.21% at 119.78 °C–178.17 °C, and the maximum decomposition rate was 135.16°C. Hashem et al^{31,32} reported that the weight loss might be due to the break of the key ion group, that is, the departure or decomposition of SeO₃²⁻. Selenopolysaccharides decompose into H₂O and SeO₂ during heating, thereby losing part of the weight. Moreover, this weight loss is related to the loss of water from the biopolymer structure.^{14,33} Figure 3C shows that the weight loss peak of Se-DCSP is steeper during heating, indicating that the selenized cornbeard polysaccharide has reduced thermal stability. Gao et al³⁴ obtained the same results.

FT-IR Spectra

Figure 4A shows the FT-IR spectra of DCSP and Se-DCSP before and after selenization, and the main characteristic absorption peaks are shown in Table 2. The absorption peaks at 3394–3400 and 2929–2931 cm⁻¹ were attributed to the stretching vibration of O-H and C-H bonds of the polysaccharide, respectively. The absorption peak at 1596–1600 cm⁻¹ corresponded to the -COOH stretching vibration in the polysaccharide. The absorption peaks at 1151 and 1030 cm⁻¹ indicate the presence of an α -glucose residue pyranosyl ring.^{35,36} The absorption bands at 842 and 917 cm⁻¹ (Se-DCSP) indicate the presence of α -glycosides and β -glycosides.³⁷

Compared with DCSP, Se-DCSP has characteristic absorption peaks of selenate at 619 and 1111 cm⁻¹, which belong to the characteristic absorption peaks of O-Se-C and O-Se-O, respectively. These peaks indicate the presence of selenate bonds in the selenized polysaccharide,³⁸ that is, the selenylation of CSP is successful.

UV–Vis Spectra

Figure 4B shows the UV–vis spectra of DCSP and Se-DCSP, and their adsorption intensities decreased with the increase of wavelength, which was consistent with the general characteristics of polysaccharides.³¹ In addition, no absorption

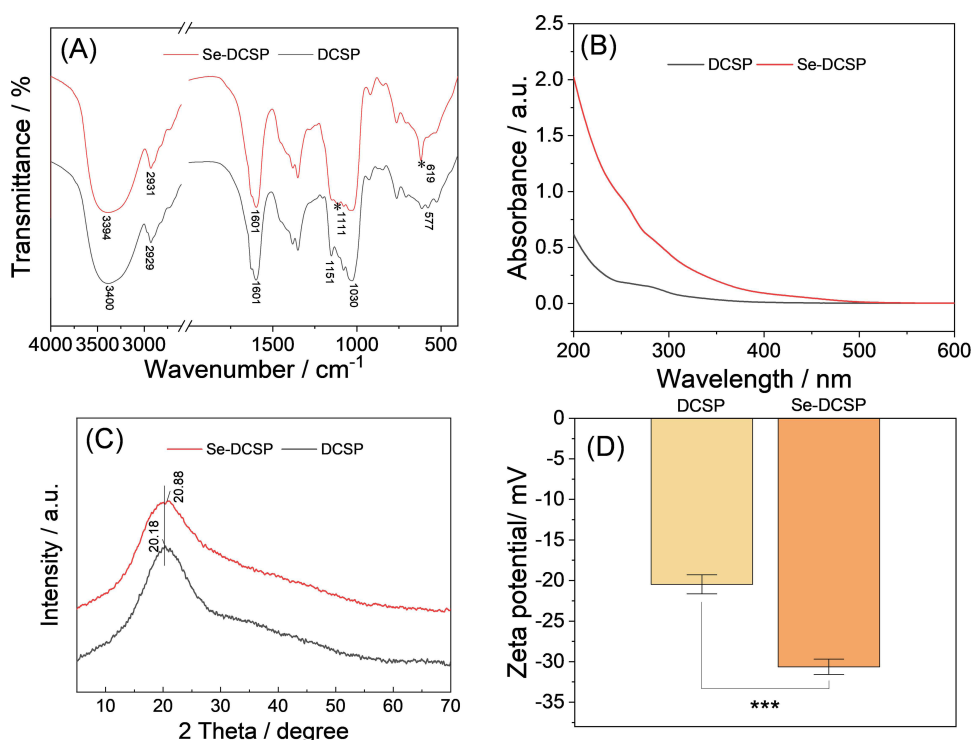


Figure 4 Characterization of DCSP and Se-DCSP. (A) FT-IR spectra; (B) UV spectra; (C) XRD spectra; (D) Zeta potential spectra. ***P<0.001.

Table 2 FT-IR Characteristic Absorption Peaks of DCSP Before and After Selenization

Sample	Selenium Content / $\mu\text{g/g}$	Characteristic Absorption Peaks of Groups / cm^{-1}					
		-OH	-COOH	-CH ₂	Sugar Ring	O-Se-C	O-Se-O
DCSP	19.5 \pm 4.9	3400	1601	2929	1030 1151	—	—
Se-DCSP	1226.7 \pm 2.4	3394	1601	2931	1032 1151	619	1111

peaks were found at 260, 280, and 520 nm, indicating that DCSP and Se-DCSP do not contain proteins, nucleic acids, and pigments.²⁹

XRD Patterns

XRD can be used to provide more structural information, such as being amorphous or crystalline.⁴ As shown in Figure 4C, the XRD patterns of DCSP and Se-DCSP showed no evident diffraction peak in the range of 5°-70° and only a broad peak appeared around 20.26°, which was related to the large and complex polymeric structure of the polysaccharide. Figure 4C indicates that DCSP and Se-DCSP are semi-crystalline or amorphous substances.³⁹ That is, selenylation did not change the crystal form of CSP.

In addition, the position of the maximum diffraction peak of Se-DCSP shifted in the direction of 2θ increase compared with DCSP, which was 20.18° for DCSP and 20.88° for Se-DCSP. This phenomenon may be due to the new chemical bond (selenite $-\text{SeO}_3^{2-}$) introducing possible stress in the structural network,⁴⁰ leading to changes in the physicochemical properties of Se-DCSP, such as tensile strength, solubility, flexibility, and swelling capacity.⁴¹

Zeta Potential

In general, the absolute value of the Zeta potential can reflect the stability of the colloidal dispersion system. A higher absolute value of Zeta potential indicates a more stable system.⁴² The Zeta potentials of DCSP and Se-DCSP are $-(20.5 \pm 1.2)$ and $-(30.6 \pm 1.0)$ mV, respectively (Figure 4D), which is attributed to the addition of $-\text{SeO}_3^{2-}$ ions to promote negative charge in Se-DCSP.³⁹ Therefore, the Se-DCSP solution is more stable and less likely to congregate or aggregate.

Monosaccharide Components Analysis

Monosaccharide standard and DCSP peak time is shown in the selenylation position of DCSP is shown in Figure 5A and B, DCSP in 8.23 min and 8.74 min and 10.99 min and 12.42 min and 38.88 min has absorption peak, compared with the standard spectrogram, found that the content of glucose (Glc) sugar is as high as 97.71%, The total proportion of other polysaccharides was less than 3%, and the specific values are shown in Table 3. The results showed that the major monosaccharide component of DCSP was glucose.

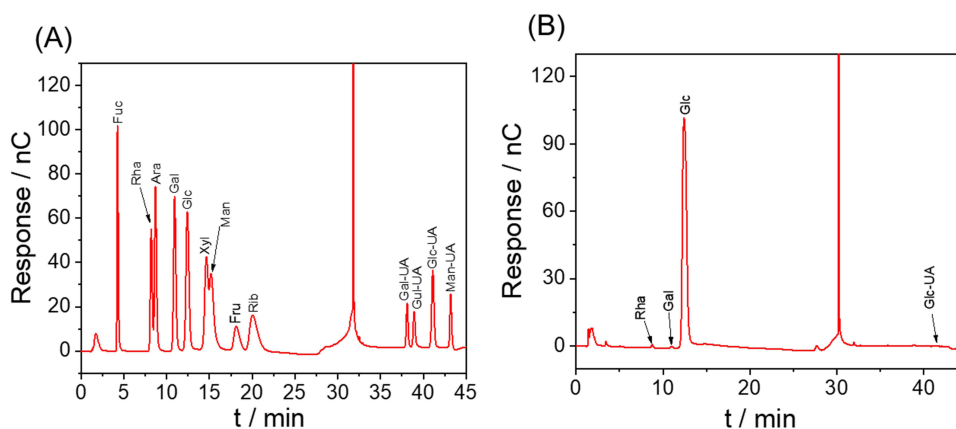
**Figure 5** Monosaccharide component determination and analysis results. (A) Standard chromatogram; (B) DCSP chromatogram.

Table 3 Monosaccharide Components of DCSP

Peak name	Retention Time / Min	Peak Area mV×Min	Monosaccharide Composition / %
Fuc	n.a.	n.a.*	0.00
Rha	8.23	0.04	0.13
Ara	8.74	0.33	0.70
Gal	10.99	0.20	0.40
Glc	12.42	56.49	97.71
Xyl	n.a.	n.a.	0.00
Man	n.a.	n.a.	0.00
Fru	n.a.	n.a.	0.00
Rib	n.a.	n.a.	0.00
Gal-UA	n.a.	n.a.	0.00
Gul-UA	n.a.	n.a.	0.00
Glc-UA	38.88	0.18	1.05
Man-UA	n.a.	n.a.	0.00

Note: *"n.a." indicates that no signal was detected.
Abbreviations: Fuc, Fucose; Rha, Rhamnose; Ara, Arabinose; Gal, Galactose; Glc, Glucose; Xyl, Xylose; Man, Mannose; Fru, Fructose; Rib, Ribose; Gal-UA, Galacturonic Acid; Gul-UA, Glucuronic Acid; Glc-UA, Guluronic Acid; Man-UA, Mannuronic Acid.

1D and 2D Nuclear Magnetic Resonance (NMR)

NMR further elucidated the structural features of DCSP. In the proton spectra of polysaccharides, chemical shifts are usually present in the range of 1.0 to 6.0 ppm, with a range of 4.3–6.0 ppm considered to be associated with anomer protons (Figure 6B and D). The region of 3.2 to 4.2 ppm is associated with protons present on C2–C6.^{43,44} Figure 6B shows the ¹H NMR spectrum of DCSP, and the end-group isomeric proton resonance exceeds 4.95 ppm, indicating the presence of α-pyranosyl,^{45,46} which is consistent with the results of infrared characterization. The backbone structure of cornbeard polysaccharide was reported to be a skeleton composed of (1→4)-α-D-Glcp and (1→4,6)-α-D-Glcp glucose.^{15,47} Based on the literature of Wang et al,¹⁸ we made a simple attribution of the ¹H-NMR and ¹³C-NMR spectra of DCSP and Se-DCSP (Tables 4 and 5), as shown in the spectra of ¹H, ¹³C, and HSQC. The five main cross-peaks of DCSP were 891.84/5.15, 95.70/4.58, 97.85/4.89, 99.57/5.34, and 102.53/4.45 ppm, which were labeled as residues A–E (Figure 6A, B, and E). The H-H COSY spectrum can obtain the coupling between ortho hydrogen atoms and hydrogen atoms, and the NOCSY spectrum can provide a complete set of hydrogen-related monosaccharide residues, and their combination can obtain the complete hydrogen on the monosaccharide residues. Based on previous reports,⁴⁷ combined with the hydrogen signal observed at δ 5.32 ppm in the HSQC spectrum and the carbon signal detected at δ 99.60 ppm, the cross-peaks of C2/H2 (71.53/3.42 ppm), C3/H3 (73.30/3.88 ppm), C4/H4 (76.69/3.58 ppm), and C5/H5 (71.16/3.75 ppm) could be further determined from COSY, NOCSY, and HSQC. The spectra were assigned, from which residue A could be determined to be (1→4,6)-α-D-Glcp. In addition, the chemical shifts corresponding to (1→4)-α-D-Glcp C1/H1 to C6/H6 at 95.78/4.58, 73.91/3.20, 72.69/3.64, 76.78/3.86, 70.36/3.67, and 73.30/3.88 ppm were observed. Another study⁴⁸ showed that the anomeric carbon signal at δ92.0 ppm could be attributed to C1 of the terminal α-D-Glcp. Moreover, based on the cross-peak, HSQC at δH/C, 102.58/4.45, 73.10/3.26, 73.36/3.68, 69.49/3.36, 72.05/3.60, and 60.47/3.72 ppm was assigned to 1→3)-β-D-Galp C1–C6.⁴⁶ Similarly, residue E was assigned to (1→3,5)-β-D-Manp.^{49,50}

The selenium-group position of polysaccharides is usually determined by ¹³C NMR spectroscopy. In the NMR carbon spectrum, nonisomeric carbon appears in the range of 60 to 85 ppm, whereas anomeric carbon appears in the range of 90 to 110 ppm.⁵¹ As shown in Figure 6C, the C-1 signal is found at 90 to 100 ppm, whereas no signal is observed at 83 to 88 ppm, indicating that most of the sugar residues of DCSP and Se-DCSP are in the form of pyran rings,⁵² which is consistent with the hydrogen spectrum.

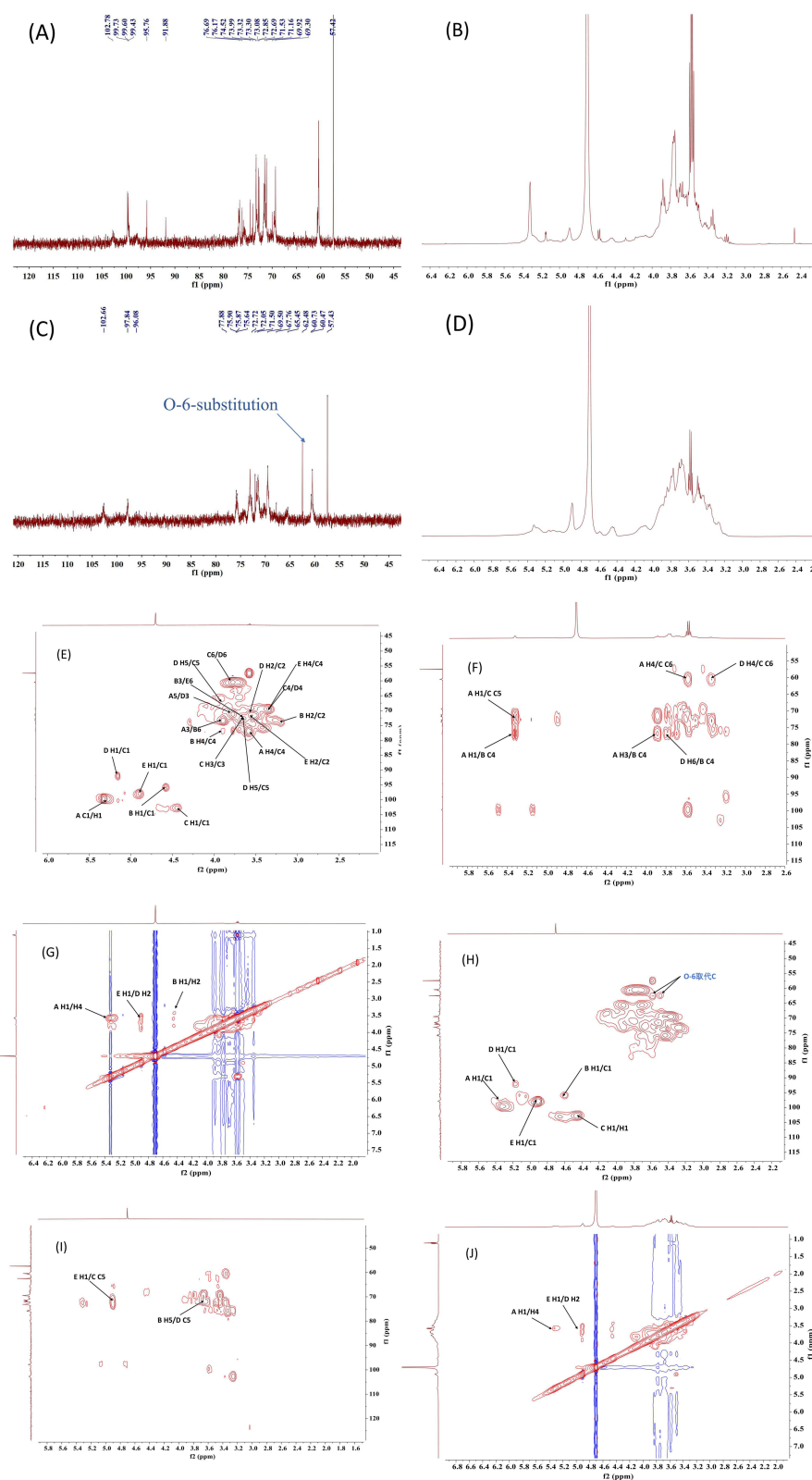


Figure 6 NMR characterization of DCSP and Se-DCSP. (A) ^{13}C -NMR spectrum of DCSP; (B) ^1H -NMR spectrum of DCSP; (C) ^{13}C -NMR spectrum of Se-DCSP; (D) Se-DCSP ^1H -NMR spectrum. (E–G) are the HSQC, HMBC and NOESY spectra of DCSP respectively; (H–J) are the HSQC, HMBC and NOESY spectra of Se-DCSP respectively. (C) The middle blue mark indicates that the new signal peak at 62.48 ppm is attributed to O-6 substituted carbon.

Table 4 Structure Characterization of DCSP by ¹³C-¹H-NMR Spectra

Residue	Chemical Shifts (δ ppm)					
	C1/H1	C2/H2	C3/H3	C4/H4	C5/H5	C6/H6
A: (1→4)-α-D-Glcp	99.60/5.32	71.53/3.42	73.30/3.88	76.69/3.58	71.16/3.75	/
B: (1→4)-α-D-Glcp	95.78/4.58	73.91/3.20	72.69/3.64	76.78/3.86	70.36/3.67	73.30/3.88
C: (1→3)- β -D-Galp	102.78/4.44	73.08/3.24	73.32/3.66	69.38/3.34	72.85/3.61	60.48/3.75
D: End of α -D-Glcp	91.88/5.15	71.28/3.51	71.16/3.75	69.38/3.34	69.92/3.91	60.48/3.77
E: (1→3,5)- β -D-Manp	97.85/4.89	71.21/3.45	76.17/3.68	69.92/3.93	72.69/3.61	73.32/3.28

Table 5 Structure Characterization of Se-DCSP by ¹³C-¹H-NMR Spectra

Residue	Chemical Shifts (δ ppm)					
	C1/H1	C2/H2	C3/H3	C4/H4	C5/H5	C6/H6
A: (1→4,6)-α-D-Glcp	99.57/5.34	71.64/3.51	73.10/3.84	76.80/3.59	71.46/3.77	/
B: (1→4)-α-D-Glcp	95.70/4.61	73.36/3.26	72.93/3.67	76.06/3.86	70.35/3.66	73.36/3.89
C: (1→3)- β -D-Galp	102.58/4.45	73.10/3.26	73.36/3.68	69.49/3.36	72.05/3.60	60.47/3.72
D: End of α -D-Glcp	92.27/5.18	71.50/3.52	71.12/3.79	69.49/3.36	69.91/3.96	60.47/3.77
E: (1→3,5)- β -D-Manp	97.85/4.92	71.05/3.43	76.16/3.68	69.91/3.96	72.93/3.67	73.36/3.28

Comparing the ¹³C-NMR spectra of DCSP and Se-DCSP, some nonisomeric carbon signals in the range of 60.39 to 76.69 ppm in DCSP were different from those in Se-DCSP. In particular, the new peak at 62.48 in Se-DCSP was due to the substitution of -SeO₂H, that is, O-6 selenization. However, the C-6 peak of Se-DCSP remained at 60.47 ppm, and this peak did not decrease significantly, indicating that the primary hydroxyl group on the medial side was not selenized.⁵³ Based on the results of ¹³C NMR, the signal intensity of the O-substituted carbon indicates that the C-6 substitution is dominant.

The HSQC (residues A-E), HMBC, and COSY spectra of Se-DCSP (Figure 6H–J) were similar to those of DCSP (Figure 6E–G), indicating that the main chain structure of the polysaccharide had not changed. However, in addition to a new peak at 62.48 ppm observed at ¹³C of Se-DCSP, a 62 ppm signal was also found on the HSQC (Figure 6H) spectrum of Se-DCSP, and these results indicate the non-selective selenization of Se-DCSP in which the C-6 substitution is dominant. The selenylation position of DCSP is shown in Figure 7.

Antioxidant Activity

The antioxidant activity of CSPs before and after selenization was compared by examining their ability to scavenge •OH, DPPH, and ABTS radicals in vitro. The results showed that DCSP and Se-DCSP increased in a concentration-dependent manner during the scavenging of the abovementioned free radicals in the tested dose range, and the selenide

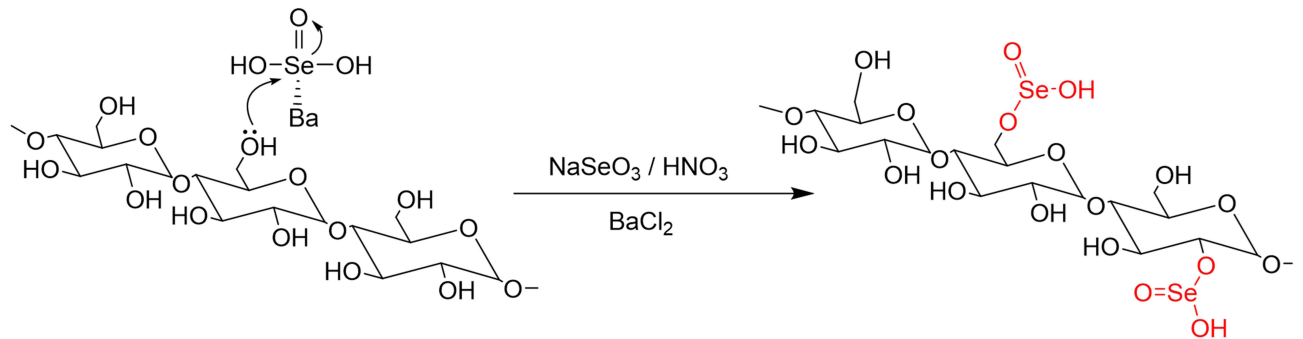


Figure 7 Structure of DCSP and its molecular formula of selenization reaction.

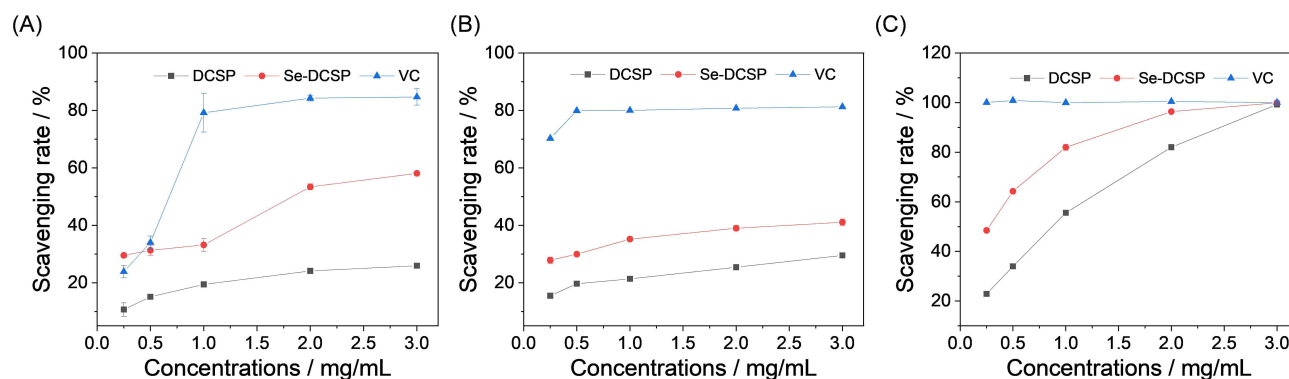


Figure 8 Comparison of antioxidant activity of DCSP and Se-DCSP. (A) $\cdot\text{OH}$ radical clearance curve; (B) DPPH free radical clearance curve; (C) ABTS free radical clearance curve.

polysaccharide had a stronger free radical scavenging ability than the original polysaccharide (Figure 8). In particular, Figure 8A shows that at 3 mg/mL, the clearance of $\cdot\text{OH}$ radicals by DCSP and Se-DCSP reached $25.9\% \pm 0.6\%$ and $58.1\% \pm 0.2\%$, respectively. Figure 8B shows that the DPPH radical scavenging of DCSP and Se-DCSP was $29.5\% \pm 0.3\%$ and $41.1\% \pm 1.1\%$, respectively, when the concentration was 3.0 mg/mL. Figure 8C shows that when the concentration of DCSP increased from 0.25 to 3 mg/mL, the ABTS scavenging ability of DCSP and Se-DCSP increased from $22.9\% \pm 0.3\%$ and $48.5\% \pm 0.5\%$ to $99.2\% \pm 0.4\%$ and $99.9\% \pm 0.1\%$, respectively. Se-DCSP has a stronger antioxidant capacity than DCSP.

Cytotoxicity of DCSP and Se-DCSP and Their Protective Effects on HK-2 Cells

The toxicity of DCSP and Se-DCSP on HK-2 cells was determined by using the CCK-8 assay (Figure 9A). After incubation with 30–120 $\mu\text{g/mL}$ of polysaccharide for 24 h, the viability of HK-2 cells was above 100%, indicating that DCSP and Se-DCSP did not have toxic effects on HK-2 cells and promoted the growth of HK-2 cells.

Protective Effect on HK-2 Cells

After treating HK-2 cells with nanoCOM for 24 h, the cell viability decreased from $100.0\% \pm 2.6\%$ to $66.4\% \pm 3.4\%$, indicating that nanoCOM crystals had evident damage to HK-2 cells.

When the cells were treated with 30, 60, 90, and 120 $\mu\text{g/mL}$ of DCSP or Se-DCSP combined with nanoCOM, the cell viability (79.69% to 94.30%) was increased to varying degrees (Figure 9B), indicating that the addition of polysaccharides could reduce the cell damage caused by nanoCOM. The concentration of 60 $\mu\text{g/mL}$ had the best protective effect.

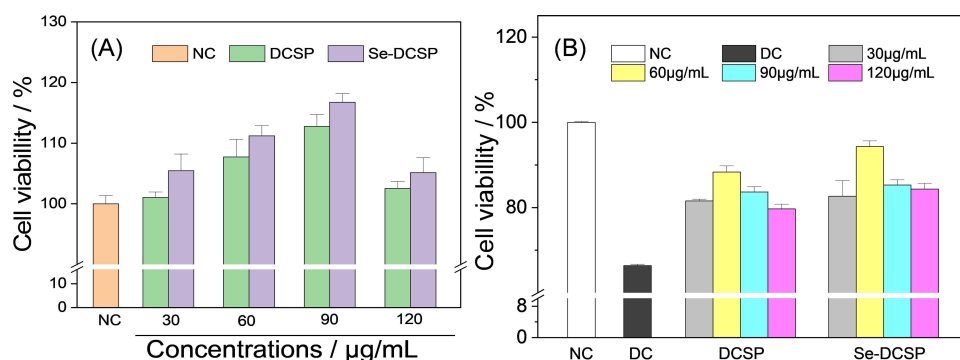


Figure 9 Cytotoxicity of DCSP and Se-DCSP (A) and protective effects on HK-2 cells (B). NC: normal control; DC: damaged control by 200 $\mu\text{g/mL}$ nanoCOM. Injury time: 24h. Polysaccharide protection time: 24h.

Cell Morphology Observed by HE Staining

As shown in [Figure 10](#), after HE staining, the cells in the normal group had a full morphology. The cell morphology of the injury group was shrunken and abnormal; the color of the nucleus was darker than that of the normal group, and the cell membrane was broken. After being protected by polysaccharides, the morphology of the cells gradually returned to normal. Among them, the state of cells protected by Se-DCSP was closest to that of normal cells.

Effect of nanoCOM on ROS Levels in HK-2 Cells Under DCSP and Se-DCSP Protection

[Figure 11](#) shows the changes in intracellular ROS levels caused by nanoCOM crystals protected by DCSP and Se-DCSP. The distribution of green fluorescence in the four groups of cells was observed by using a confocal laser scanning microscope after the intracellular ROS was stained with DCFH-DA. The results showed that the fluorescence intensity of the normal group was weak, and almost no green fluorescence was observed. However, the fluorescence intensity of the injured group was relatively strong, and many cells had evident morphological shrinkage (red arrow in [Figure 11A](#)).

After protection with DCSP or Se-DCSP, the fluorescence intensity of the protection group was significantly lower than that of the injury group, and the number of cells with shrinkage was significantly reduced. Moreover, the inhibition of Se-DCSP on the increase of intracellular ROS level caused by nanoCOM was stronger than that of DCSP.

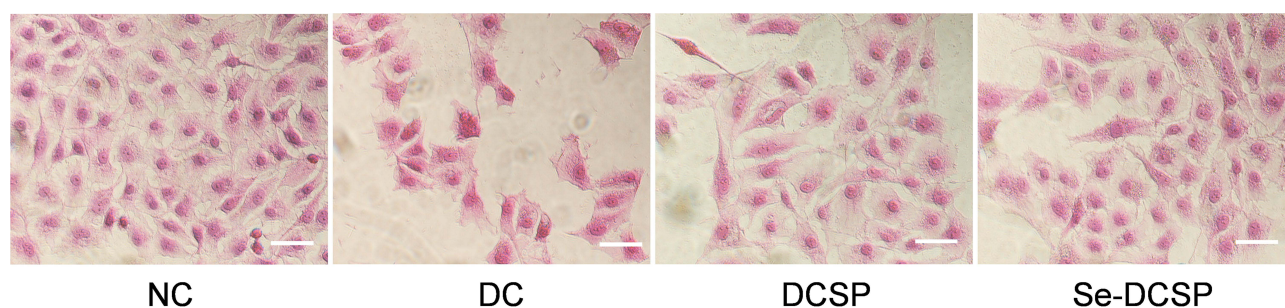


Figure 10 Effect of nanoCOM crystals protected by Se-DCSP and DCSP on the morphology of HK-2 cells. NC: normal control; DC: damaged control by 200 $\mu\text{g/mL}$ nanoCOM. Injury time: 24h. Polysaccharide concentration: 60 $\mu\text{g/mL}$. Polysaccharide protection time: 24 h. Scale bar: 20 μm .

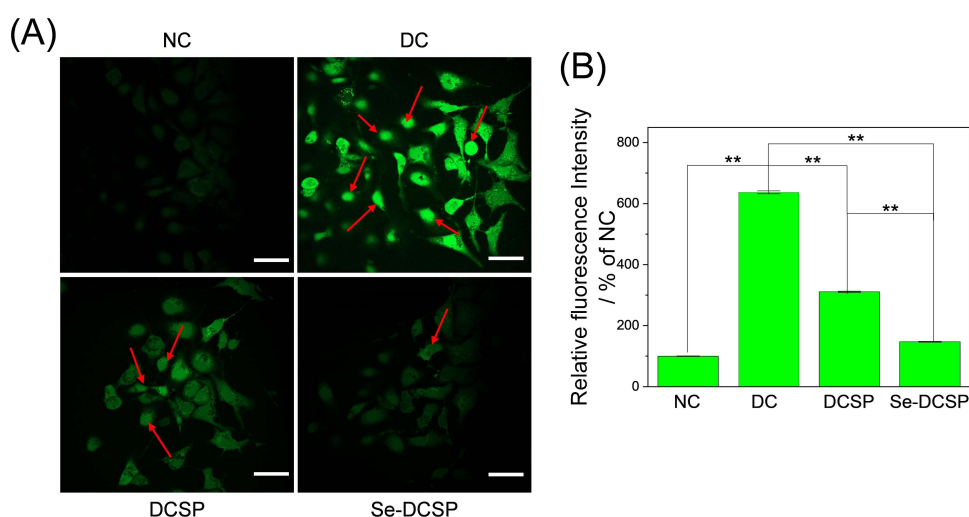


Figure 11 Effect of nanoCOM on ROS level in HK-2 cells under the protection of DCSP and Se-DCSP. (A) ROS fluorescence image, the red arrows point to cells with representative ROS levels; (B) ROS semi-quantitative histogram. NC: normal control; DC: damaged control by 200 $\mu\text{g/mL}$ nanoCOM. Injury time: 24h. Polysaccharide concentration: 60 $\mu\text{g/mL}$. Polysaccharide protection time: 24 h. Scale bar: 20 μm . ** $P < 0.01$.

Qualitative and Quantitative Detection of Mitochondrial Membrane Potential Changes

The changes in the mitochondrial membrane potential of HK-2 cells before and after polysaccharide protection were observed by laser confocal microscopy using the cationic lipophilic dye JC-1 as a fluorescent probe (Figure 12A and C).

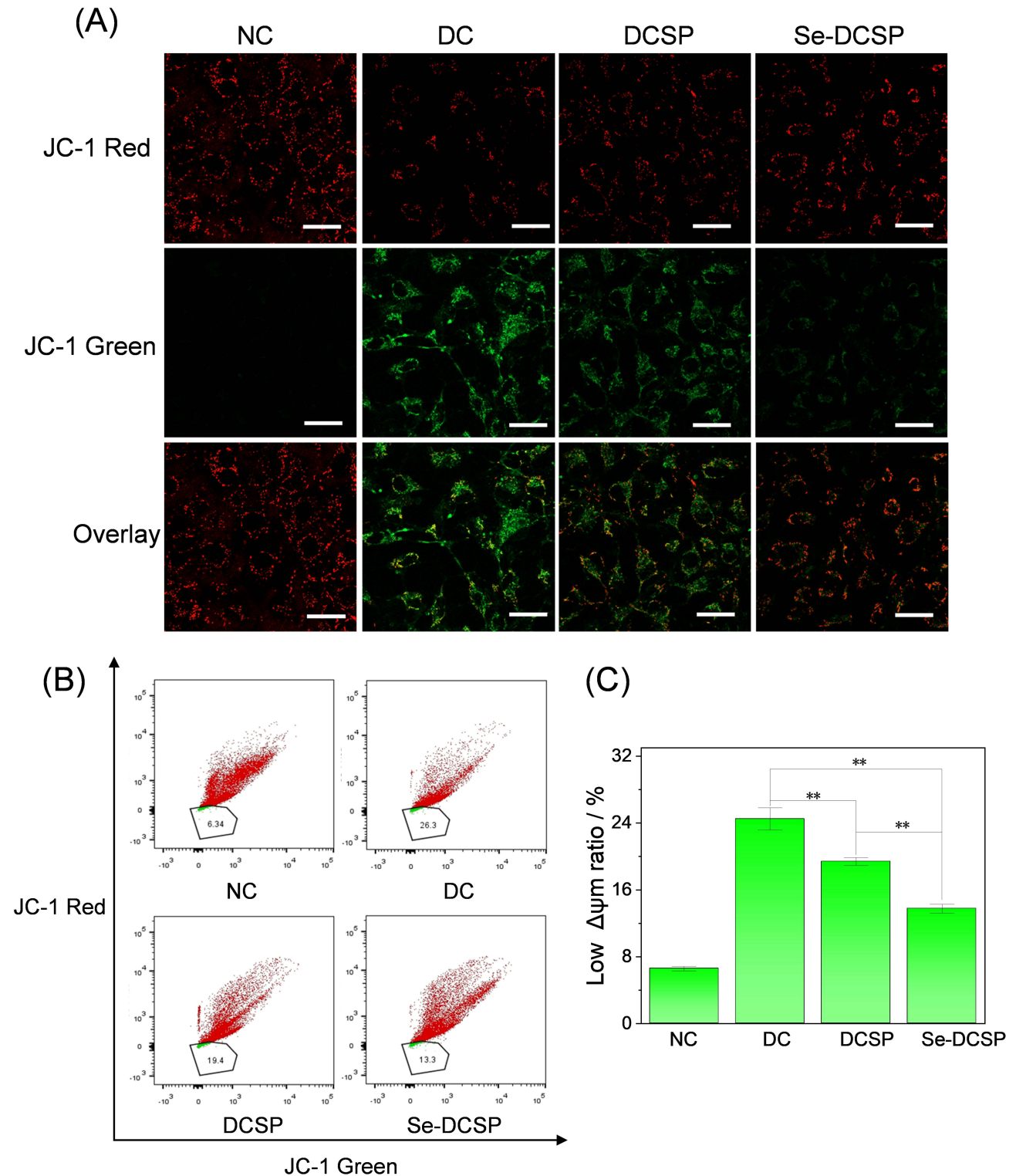


Figure 12 Effect of nanoCOM crystals on mitochondrial membrane potential of HK-2 cells under the protection of Se-DCSP and DCSP (A) observation by confocal microscope; (B) Scatter plot by flow cytometry; (C) Quantitative analysis of JC-1 histogram. NC: normal control. DC: damaged control by 200 μ g/mL nanoCOM. Injury time: 24h. Polysaccharide concentration: 60 μ g/mL. Polysaccharide protection time: 24 h. Scale bar: 20 μ m. **P<0.01.

In normal cells, almost no green fluorescence was observed, that is, the mitochondrial membrane potential was high, and JC-1 was all accumulated in the matrix of the mitochondria, forming polymers and emitting red fluorescence. However, nanoCOM-damaged cells showed strong green fluorescence and weak red fluorescence, indicating low membrane potential. Under the protection of Se-DCSP and DCSP, the green fluorescence intensity of cells was weaker than that of the injury group, and the red fluorescence was stronger than that of the injury group, that is, the mitochondrial membrane potential of cells was increased after the protection of polysaccharides, and the protective effect of Se-DCSP was better than that of DCSP.

Flow cytometry (Figure 12B) showed that the proportion of cells with low potential (green fluorescence) in the NC group was 6.34%, and that in the nanoCOM injury group increased to 26.3%, indicating that the mitochondrial membrane potential of the cells in the injury group decreased. The percentage of low potential (green fluorescence) in DCSP and Se-DCSP groups was 19.4% and 13.3%, respectively, indicating that the mitochondrial membrane potential of cells protected by polysaccharides increased, which was consistent with the results obtained by the abovementioned methods.

Expression of Monocyte Chemoattractant Protein-1 (MCP-1)

Inflammation is an important link in the formation of intrarenal crystals. MCP-1 is an important inflammatory factor in kidney stone formation.⁵⁴ Laser confocal microscopy was used to observe the changes in MCP-1 expression before and after polysaccharide protection (Figure 13). The weak green fluorescence in the normal cell group indicated that the MCP-1 content was low. However, the green fluorescence of nanoCOM-damaged cells became bright, indicating that the expression of MCP-1 was significantly increased. Among them, the proportion of green fluorescence in the normal group was 2.42%, whereas the proportion of green fluorescence in the injury group was as high as 8.41%. Compared with the nanoCOM damage group, the green fluorescence of the nanoCOM damage group was weakened by DCSP and Se-DCSP (5.66% and 3.46%, respectively), and the Se-DCSP group was close to the normal group, indicating that the anti-inflammatory effect of the selenized polysaccharide was stronger than that of the pre-selenized polysaccharide.

Expression of NLRP3

The NLRP3 inflammasome is a cytosolic signaling complex that mediates the activation of potent inflammatory mediators and has been implicated in the pathogenesis of many common noncommunicable diseases.⁵⁵ The activation of NLRP3 leads to the assembly of inflammasome, induces the activation of the cytokine interleukin-1 β (IL-1 β) mediated by caspase 1, and promotes the occurrence of inflammatory pyroptosis.

The expression of NLRP3 in HK-2 cells before and after polysaccharide protection was observed by confocal microscopy. As shown in Figure 14, the intensity of green fluorescence of NLRP3 expression in the nanoCOM injury group was significantly stronger than that in normal cells, indicating that nanoCOM induced the activation of NLRP3 inflammasome. Compared with the nanoCOM injury group, the green fluorescence of DCSP and Se-DCSP protection groups was weakened in varying degrees, and the Se-DCSP group had the best effect, which tended to be close to the normal group, indicating that Se-DCSP protection had better anti-inflammatory performance.

Content of Nitric Oxide (NO)

NO is a signaling molecule that plays a key role in the pathogenesis of inflammation, and it has anti-inflammatory effects under normal physiological conditions.⁵⁶ NO is considered as a proinflammatory mediator that induces inflammation caused by overproduction under abnormal conditions, with small amounts (picomoles) of NO being physiologic and protective and large amounts (micromoles) of NO being proinflammatory and harmful.⁵⁷

The level of NO in each group of cells detected by the DAF-FM DA fluorescent probe is shown in Figure 15. The cells in the normal group had almost no fluorescence. By contrast, the cells in the nanoCOM damage group showed intense green fluorescence (Figure 15A), indicating that NO was at a high level. Among them, the fluorescence intensity of the nanoCOM damage group was 2.5 times that of the normal group (Figure 15B). After polysaccharide protection, the fluorescence intensity of NO in the cells decreased to different degrees, among which the fluorescence intensity of the Se-DCSP protection group was closest to that of the normal group, indicating that Se-DCSP could effectively reduce NO production in the cells and maintain NO content in the normal physiological range.

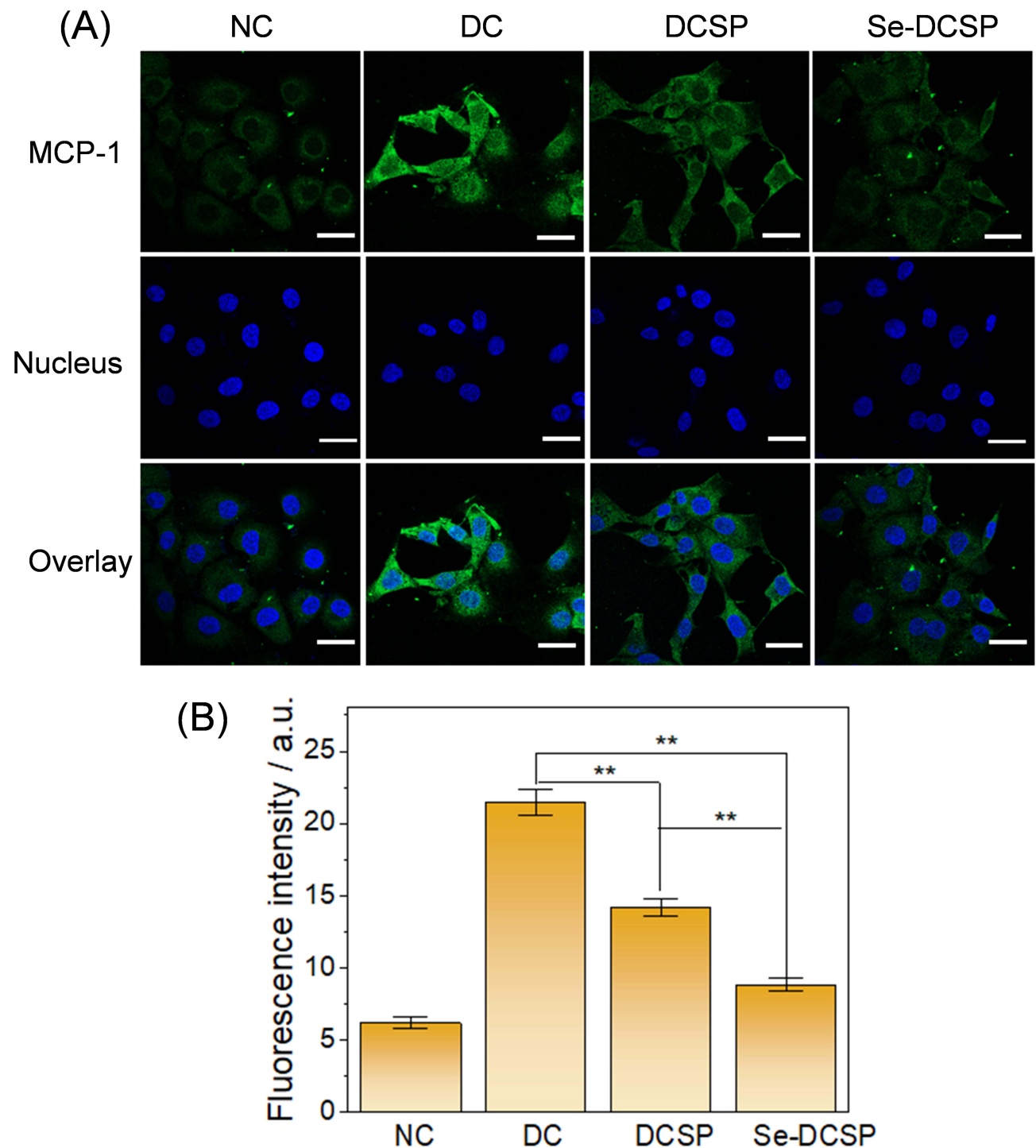


Figure 13 (A) Laser confocal observation of polysaccharide before and after selenization inhibited the expression of MCP-1 in HK-2 cells induced by nanoCOM and **(B)** quantitative analysis of MCP-1 histogram. MCP-1 shows green fluorescence, and the cell nucleus shows blue fluorescence. NC: normal control. DC: damaged control by 200 $\mu\text{g/mL}$ nanoCOM. Injury time: 24h; Polysaccharide concentration: 60 $\mu\text{g/mL}$. Polysaccharide protection time: 24 h. Scale bar: 20 μm . ** $P < 0.01$.

Discussion

Selenoylation of DCSP and Changes in Properties Before and After Selenoylation

As the main active component of corn silk, polysaccharides have attracted increasing attention because of their unique pharmacological properties and biological activities such as anti-oxidation, anti-diabetes, and anti-glycation.⁵⁸ However,

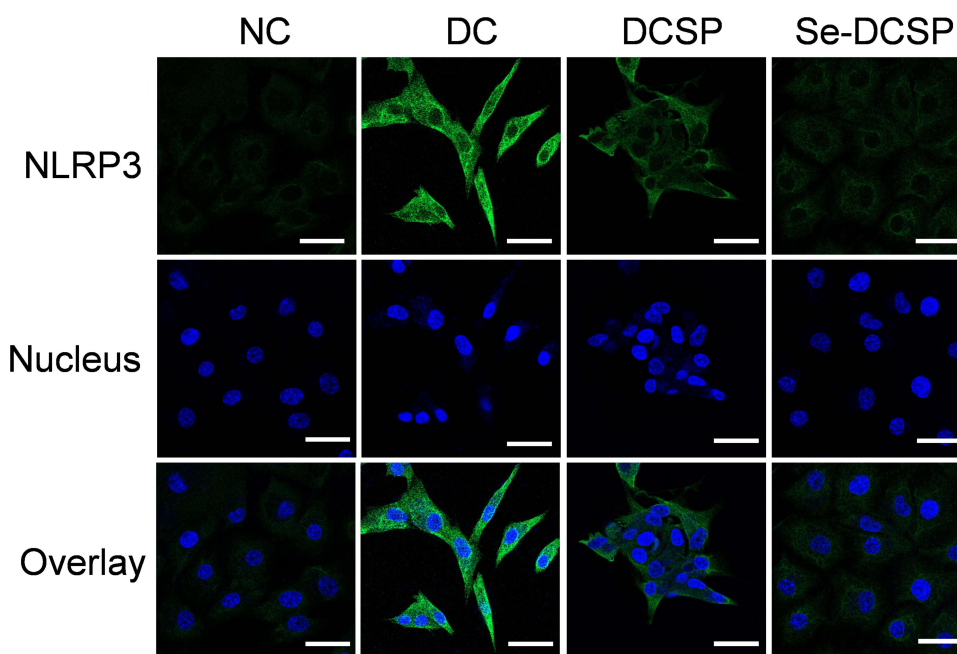


Figure 14 Laser confocal observation of polysaccharide inhibiting the expression of NLRP3 in HK-2 cells induced by nanoCOM before and after selenization. NC: normal control; DC: damaged control by 200 $\mu\text{g/mL}$ nanoCOM. Injury time: 24h. Polysaccharide concentration: 60 $\mu\text{g/mL}$. Polysaccharide protection time: 24 h. Scale bar: 20 μm .

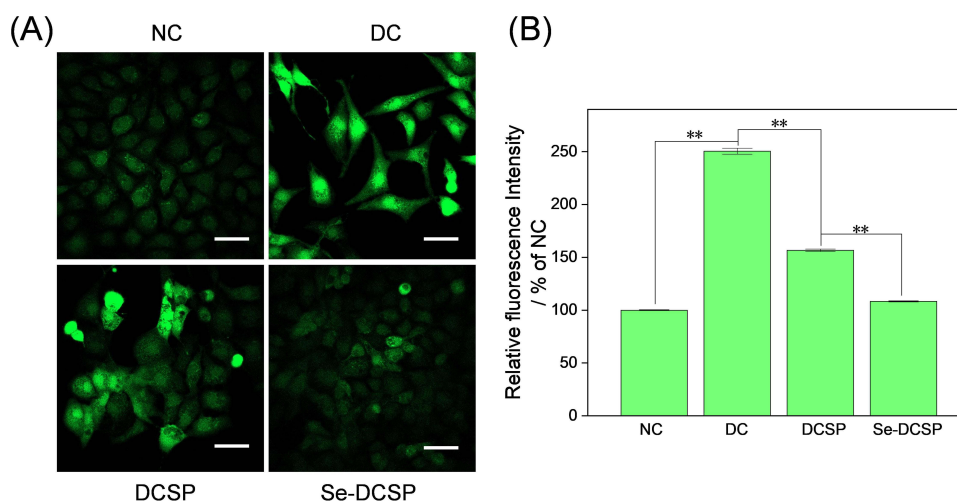


Figure 15 Laser confocal observation of polysaccharide inhibiting the expression of NO in HK-2 cells induced by nanoCOM before and after selenization. (A) NO fluorescence chart; (B) NO fluorescence intensity quantitative histogram. Scale bar: 50 μm . ** $P < 0.01$.

natural CSPs have relatively low activity. The chemical modification of natural polysaccharides has greatly improved the activity of polysaccharides and their application potential in food, medicine, materials, and other fields.

In this study, DCSP was selenized by using the $\text{HNO}_3\text{-NaSeO}_3$ method, and Se-DCSP with a selenium content of 1227 $\mu\text{g/g}$ was obtained. The structure of the polysaccharide was determined by using the FT-IR, Zeta, and NMR methods. In addition, NMR analysis confirmed that selenylation did not change the glycosidic bonds and sugar residues. Se-DCSP residues contain (1 \rightarrow 4)- α -D-Glcp, (1 \rightarrow 4,6)- α -D-Glcp, (1 \rightarrow 3)- β -D-Galp, end of α -D-Glcp, and (1 \rightarrow 3,5)- β -D-Manp. This structure is similar to that of CSP elucidated by Guo et al.⁴⁷ and Singh et al.¹⁵

XPS analysis showed that compared with DCSP, Se-DCSP showed two new peaks at 165.88 and 60.73 eV, corresponding to Se 3p_{3/2} and Se 3d peaks, respectively, indicating that the selenium group is a form of selenite. The characteristic FT-IR peaks of Se-DCSP at 619 and 1111 cm^{-1} were attributed to the stretching vibration of O-Se-C and

O-Se-O, respectively, and the new peak of ^{13}C NMR at 62.48 ppm was assigned to the O-6-replaced carbon. These results indicated that DCSP was successfully selenized.

The results showed that Se-DCSP has smaller Mw, more negative Zeta potential, and stronger antioxidant and anti-inflammatory ability than DCSP, which can effectively protect HK-2 cells from nanoCOM-induced damage, reduce ROS production, increase mitochondrial membrane potential, and inhibit kidney stone formation.

Antioxidant Comparison Between Se-DCSP and DCSP

Enhancement of the Antioxidant Capacity of Polysaccharides

The results show that Se-DCSP has stronger scavenging ability of hydroxyl free radical, DPPH free radical, and ABTS free radical than DCSP. Selenization can enhance the antioxidant ability of polysaccharides because of the following aspects: First, the presence of the $-\text{OSeO}_2\text{H}$ group in Se-DCSP molecules can activate the hydrogen atom of the hetero-carbon and increase the hydrogen supply capacity of polysaccharides.⁵³ Second, hydroxyl radical can be generated by Fenton reaction ($\text{Fe}^{2+} + \text{H}_2\text{O}_2 \rightarrow \text{Fe}^{3+} + \text{OH}^- + \text{OH}^\bullet$), which can easily react with biomolecules and cause oxidative damage.⁵⁹ The $-\text{OSeO}_2\text{H}$ group present in Se-DCSP can chelate metal ions (Fe^{2+} or Cu^{2+}) to inhibit the generation of hydroxyl radicals.⁵³ Meanwhile, $-\text{OSeO}_2\text{H}$, as an electron-withdrawing group, can promote the breakage of O-H bonds on the sugar ring, thereby increasing the ability of polysaccharide to capture free radicals.⁶⁰

The experimental results also support the idea that selenization can enhance polysaccharide activity. Liu et al⁶¹ reported that Se-APS2 and Se-APS3 with 1.05 and 2.57 $\mu\text{g}/\text{mg}$ of selenium, respectively, exhibited 88.1% and 92.0% DPPH and 45% and 42% ABTS free radical antioxidant activities, which are significantly higher than non-selenized polysaccharides (45% DPPH and 25% ABTS free radical antioxidant activities, respectively). Hou et al⁶² showed that selenized atractylodes polysaccharides showed higher DPPH, ABTS, and hydroxyl radical scavenging abilities ($p < 0.05$). Li et al⁶³ found that the selenized *Grifola frondosa* polysaccharide SeGFP2 had good antioxidant capacity.

As can be seen from Figure 8, the ability of polysaccharides to clear $\cdot\text{OH}$ and DPPH free was not very strong. Li et al⁶⁴ showed through quantitative structure activity relationship models that the contents of arabino saccharide and galacturonic acid were positively correlated with the ability of polysaccharides to scavenge $\cdot\text{OH}$ and DPPH free radicals.⁶⁵ Due to the low content of arabinose and galactose contained in DCSP (0.7% and 0.4%), therefore, the scavenging ability of DCSP on $\cdot\text{OH}$ and DPPH free radicals was weak, but the scavenging ability of polysaccharides after selenization was improved.

Reduction of Oxidative Damage in Cells

nanoCOM crystals can damage HK-2 cells, release a large amount of ROS, and reduce the mitochondrial membrane potential $\Delta\Psi\text{m}$. The injured cells can activate NADPH oxidase,⁶⁶ cause mitochondrial dysfunction, produce ROS, induce oxidative stress, and promote the opening of mitochondrial permeability transition pore, which leads to the increase of mitochondrial inner membrane permeability and the release of Ca^{2+} from the mitochondrial matrix, and the loss of Ca^{2+} forces the mitochondrial depolarization membrane potential. Finally, this phenomenon caused the decrease of mitochondrial membrane potential.⁶⁷ In this process, ROS was overproduced, leading to the disruption of homeostasis⁶⁸ and damage to cellular components such as lipids, proteins, and DNA. Long-term high levels of ROS can lead to severe cell damage and even death.⁶⁹ Zhan et al⁷⁰ showed that selenized cherry pulp polysaccharide (Se-PPRLMF-2) could significantly reduce ROS and malondialdehyde (MDA) levels in erythrocytes induced by nitrogen-containing compounds in a dose-dependent manner. In this study, with the protection of Se-DCSP, the ROS level was significantly decreased, and $\Delta\Psi\text{m}$ was greatly restored, indicating that Se-DCSP could better protect cells and normalize their overall state.

Studies have confirmed that the biological activity of polysaccharides is closely related not only to its primary structure (including degree of branching, monosaccharide composition, molecular weight and number of glucoside bonds, etc.), but also to its morphology.⁷¹ Qiu et al⁷² found that ultrasonic degradation not only reduced the microscopic particle size of *Auricularia auricula* polysaccharide, but also transformed its surface roughness and microstructure into aggregates or synaptic-like filaments with reduced network connectivity, which contributed to the improvement of its antioxidant activity to a certain extent. After selenization, the form of corn silk polysaccharide changed from lumps to spherical particles, and the particle size decreased, which could improve its biological activity to a certain extent. Xu

et al⁷³ also confirmed that the improvement of thermal stability, blood lipid lowering and antioxidant activity of *Ganoderma lucidum* polysaccharide may be partly attributed to the reduction of particle size caused by ultrasonic degradation, and the microstructure changed from irregular lumps to granules.

Polysaccharides mainly enter the urine to play the role of stone prevention. Odland et al⁷⁴ studied the distribution of tritiated sulfate pentose polysaccharide distribution (PPS) in rats after intravenous injection (5 mg/kg b.wt.) for 1 h. Places in the body with high concentrations of polysaccharides include the urinary tract, urine, and the lining of the pelvis, ureters, and bladder. Xia et al⁷⁵ used FITC-labeled *Lycium barbarum* polysaccharide (FITC-LBP) to intragastric administration to rats (50 mg/kg) for 72 h. Although most of the FITC-LBP was in the feces, there was still a part of FITC-LBP in the urine, and the concentration reached the peak after 4 h and gradually decreased from 4 h to 24 h. Tostes et al⁷⁶ implanted 15 mg CaOx stones into the bladder of male Wistar rats weighing 250 g, and then treated with daily intratibial injection of low-molecular weight glucan sulfate, indicating that polysaccharide can reach the kidney and play a role in the prevention and treatment of kidney stones. That is, in addition to directly excreting into the urine to inhibit kidney stones, polysaccharides can also protect renal tubule epithelial cells from oxidative damage through their antioxidant effects.

Comparison of the Anti-Inflammatory Activity Between Se-DCSP and DCSP

Inflammation in kidney stone disease can be either an upstream (as a causative factor) or a downstream (as a complication) event. The results of clinical and experimental studies have shown that the expression levels of genes related to inflammation, immunity, and complement activation pathways increased in renal tissues of experimental animals and patients with stones.⁷⁷ Our previous studies⁷⁸ have shown that CaOx crystals, particularly nanoCOM, severely damage renal epithelial cells and release large amounts of ROS, whereas ROS overexpression induces oxidative DNA fragmentation and activates NLRP3 inflammasome, leading to elevated levels of proinflammatory cytokines MCP-1, IL-6, and IL-1 β . In addition, inducible nitric oxide synthase (iNOS) catalyzes the synthesis of a large amount of NO,^{79,80} which further strengthens tissue inflammatory damage.⁵⁷ The interaction between cellular inflammation and oxidative stress leads to tissue damage, kidney injury, and interstitial fibrosis.

A large number of studies have shown that polysaccharides have good anti-inflammatory effects. Sang et al⁸¹ showed that BSGLP could inhibit inflammation induced by high-fat diet, which was specifically manifested as the reduction of inflammatory factors (TNF- α , IL-1 β , and MCP-1) in serum and adipose tissue. Liu et al⁸² found that acidic polysaccharide (AP1-b) isolated from lignified okra could inhibit the LPS-induced inflammatory injury of RAW 264.7 cells by inhibiting the secretion of NO and reducing the levels of pro-inflammatory factors (IL-1 β , iNOS, and TNF- α). In addition, AP1-b inhibited the phosphorylation level of I κ B and p65 proteins, suggesting that the anti-inflammatory activity of AP1-b may be related to the inhibition of the NF- κ B signaling pathway. In this study, polysaccharides could effectively inhibit the damage of nanoCOM on renal epithelial cells and the inflammatory response induced by nanoCOM. Compared with the nanoCOM injury group, the secretion of NO and the expression of MCP-1 and NLRP3 in the polysaccharide protection group were decreased, and Se-DCSP had a better protective effect than DCSP, indicating a greater degree of inhibition of inflammatory factor production. Lee et al⁸³ found that the selenized elm pectin polysaccharide Se-PPU reduced LPS-induced NO production by inhibiting the protein expression of iNOS in RAW 264.7 cells. Studies have shown that Se-APS⁸⁴ can effectively ameliorate CCl₄-induced hepatocyte necrosis and inflammation, as well as significantly reduce the levels of aspartate aminotransferase, alanine aminotransferase, and MDA and the expression level of Kupffer cell-specific biomarkers CD68 and pro-inflammatory cytokines such as IL-1 β and TNF- α ($P < 0.01$).

Causes of the Enhanced Activity of Selenopolysaccharides

The biological activity of polysaccharides is related to its selenium content, monosaccharide composition, Mw, and glycosidic linkage.⁴² The present study confirmed that selenophosphorus polysaccharides formed by combining selenium with polysaccharides exhibited better antioxidant and anti-inflammatory activities than natural polysaccharides.

Causes of the Enhanced Antioxidant Activity of Selenopolysaccharides

Selenylation modification not only forms a covalent bond between selenium and polysaccharide, but also changes the properties of the polysaccharide. In general, polysaccharides with a large M_w have a relatively tight structure, large steric hindrance, and relatively few exposed active groups, which make them difficult to exert their biological effects through the cell membrane barrier.⁸⁵ However, polysaccharides with a low M_w can exert their biological activities better. In this study, the selenization of cornbeard polysaccharides was carried out under acidic conditions and high temperature, which resulted in glycan fragmentation and M_w reduction (from 15.8 kDa to 12.0 kDa). Of course, it is not that the smaller the molecular weight of the polysaccharide, the more active it is. Polysaccharide needs a certain structure to form active space when exerting its bioactivity. In general, the molecular weight of polysaccharides must be above 2000 Da to show biological activity.²³

In addition, given the introduction of selenite, the potential value of Se-DCSP is more negative. The increase of negative charge leads to the enhancement of the repulsion among polysaccharide particles, which increases its solubility and anti-aggregation ability, and enhances the antioxidant ability of the polysaccharide to a certain extent. Wei et al⁵³ synthesized a series of selenide polysaccharides (Se-RHP) from *Radix Hedysari*, whose selenium content increased from 1.04 to 3.29 mg/g, and whose M_w decreased from 62.7 to 27.7 kDa. Compared with the original *Hedysari* polysaccharide (RHP), Se-RHP exhibited better free radical scavenging activity and reducing ability in water. But it does not mean that the smaller the molecular weight of the polysaccharide, the higher its activity.

The antioxidant activity of polysaccharides depends on their hydrogen supply capacity. The introduction of selenium leads to the weakening of hydrogen bond dissociation energy and the enhancement of hydrogen supply capacity.⁶⁰ Therefore, high Se content generally enhances the biological activity of selenopolysaccharides. Wang et al⁴ also obtained a similar conclusion. Similarly, Se-containing derivatives from *Artemisia*⁸⁶ and *Potentilla anserina* L.⁸⁷ have been suggested to enhance antioxidant activity compared with natural polysaccharides. The proposed mechanism may involve a change in the conformational structure of the polysaccharide and the increase in the number of hydroxyl groups, thereby affecting the antioxidant activity. However, not all selenopolysaccharides are conducive to improving their biological activities. Studies have shown that selenized *Glycyrrhiza* polysaccharide have destructive effects on the cell membrane of many organisms.⁸⁸

Causes of the Enhanced Anti-Inflammatory Activity of Selenopolysaccharides

Oxidative stress of renal tubular epithelial cells is closely related to inflammation in the formation of kidney stones. Inflammation mediated by cell-crystal interactions can lead to inflammatory injury of renal cells, promote the intracellular expression of NADPH oxidase, and induce the extensive production of ROS. This inflammation not only promotes oxidative stress, but also activates NLRP3 inflammasome, releases a large number of inflammatory factors, initiates inflammatory cascade reaction, and promotes the aggregation, nucleation, and growth of calcium oxalate crystals. This process leads to the development of intrarenal crystal deposition and even stones.⁸⁹

On the one hand, the enhancement of the anti-inflammatory activity of polysaccharide selenide is related to the enhancement of the antioxidant activity of polysaccharide selenide, and on the other hand, such an enhancement may be related to selenium. Many studies have shown that the anti-inflammatory activity of natural polysaccharides has been improved after chemical modifications such as selenization and selenium enrichment. Hamid et al¹¹ showed that the histopathological examination of rat liver tissue confirmed that *Astragalus* selenide polysaccharide could reduce the inflammation and necrosis of liver cells caused by CCl_4 .

Polysaccharides are increasingly used as additives to improve and modify the texture, flavor, character, and nutrition of foods due to the properties of non-toxicity, wide availability and health-promoting effects.⁹⁰ He et al⁹¹ demonstrated that the addition of blackberry polysaccharide can improve the quality of boiled chicken breast, due to its ability to inhibit fat oxidation and reduce the Maillard reaction of proteins. Based on this study, Se-DCSP is expected to be used as an additive to prevent stone occurrence or delay stone recurrence.

In this paper, the anti-inflammatory activity of polysaccharide was improved by selenization modification. However, there are also study⁸⁸ that the bioactivity of polysaccharides is not significantly improved or even decreased by selenization. In future studies, we will focus on the mechanism analysis, theoretical calculation and molecular docking

work, and pay more attention to the molecular structure of polysaccharides, in order to clarify the reason why selenization improves the anti-inflammatory activity of corn wool polysaccharide.

Conclusions

In this paper, DCSP was selenized. The selenium content of Se-DCSP was significantly increased from 19.5 µg/g (DCSP) to 1227 µg/g. By selenization modification, the Mw of polysaccharides decreased, and the surface morphology changed from massive to dispersed spherical. Se-DCSP exhibited higher DPPH, ABTS, and hydroxyl radical scavenging activities than DCSP. Se-DCSP can protect renal epithelial cells from nanoCOM damage to a certain extent, reduce ROS production, and mitochondrial membrane potential, as well as downregulate the expression level of inflammatory factors MCP-1, NO, and NLRP3, which are beneficial to reduce the risk of kidney stone formation. Based on this study, Se-DCSP is expected to be used as additives as an effective ingredient in daily food and health care products to prevent the occurrence of kidney stones.

Data Sharing Statement

All the data supporting the results were shown in the paper and can be applicable from the corresponding author.

Acknowledgment

This work was supported by the National Natural Science Foundation of China (No. 82270800) and Guangdong Key Laboratory of Urology. Yu-Yun Zheng and Xin-Yi Tong are co-first authors of the article.

Disclosure

The authors declare that they have no competing interests.

References

1. Chaiyarit S, Phuangkham S, Thongboonkerd V. Quercetin inhibits calcium oxalate crystallization and growth but promotes crystal aggregation and invasion. *Curr Res Food Sci*. 2024;8:100650. doi:10.1016/j.crfs.2023.100650
2. Sivaguru M, Saw JJ, Wilson EM, Lieske JC, Krambeck AE. Human kidney stones: a natural record of universal biomineralization. *Nat Rev Urol*. 2021;18(7):404–432. doi:10.1038/s41585-021-00469-x
3. Sun XY, Zhang H, Deng JW, Yu B-X, Zhang Y-H, Ouyang J-M. Regulatory effects of damaged renal epithelial cells after repair by porphyra yezoensis polysaccharides with different sulfation degree on the calcium oxalate crystal–cell interaction. *Int J Nanomed*. 2021;16:8087. doi:10.2147/IJN.S320278
4. Wang L, Li L, Gao J, Huang J, Yang Y, Xu Y. Characterization, antioxidant and immunomodulatory effects of selenized polysaccharides from dandelion roots. *Carbohydr Polym*. 2021;260:117796. doi:10.1016/j.carbpol.2021.117796
5. Li M, Qiu L, Ai X, et al. Effects of selenium and cadmium on human liver and kidney functions in exposed black shale areas. *GeoHealth*. 2024;8(4):e2024GH001040. doi:10.1029/2024GH001040
6. Lai H, Nie T, Zhang Y, et al. Selenium deficiency-induced damage and altered expression of mitochondrial biogenesis markers in the kidneys of mice. *Biol Trace Elem Res*. 2021;199:185–196. doi:10.1007/s12011-020-02112-z
7. Wang Y, Wu Y, Luo K. The protective effects of selenium on cadmium-induced oxidative stress and apoptosis via mitochondria pathway in mice kidney. *Food Chem Toxicol*. 2013;58:61–67. doi:10.1016/j.fct.2013.04.013
8. Huang S, Chen F, Cheng H, Huang G. Modification and application of polysaccharide from traditional Chinese medicine such as *Dendrobium officinale*. *Int J Biol Macromol*. 2020;157:385–393. doi:10.1016/j.ijbiomac.2020.04.141
9. Ahmad MM. Recent trends in chemical modification and antioxidant activities of plants-based polysaccharides: a review. *Carbohydr Polym Tech Appl*. 2021;2:100045.
10. Sun X, Yu Z, Luo H, Yang Y. Selenium-containing polysaccharide-protein complex in Se-enriched *Ulva fasciata* induces mitochondria-mediated apoptosis in A549 human lung cancer cells. *Mar Drugs*. 2017;15(7):215–225. doi:10.3390/md15070215
11. Hamid M, Liu D, Abdulrahim Y. Amelioration of CCl₄-induced liver injury in rats by selenizing *Astragalus* polysaccharides: role of proinflammatory cytokines, oxidative stress and hepatic stellate cells. *Research in Veterinary Science*. 2017;114:202–211. doi:10.1016/j.rvsc.2017.05.002
12. Huang F, Sun XY, Ouyang JM. Preparation and characterization of selenized *Astragalus* polysaccharide and its inhibitory effect on kidney stones. *Mater Sci Eng C*. 2020;110:110732. doi:10.1016/j.msec.2020.110732
13. Liu Y, Xu H, Zhong W, Shen Q, Zhuang T, Huang K. Organic selenium alleviated the formation of ethylene glycol-induced calcium oxalate renal calculi by improving osteopontin expression and antioxidant capability in dogs. *Biol Trace Elem Res*. 2015;168:392–400. doi:10.1007/s12011-015-0373-9
14. Wans EM, Ahmed MM, Mousa AA, Tahoun EA, Orabi SH. Ameliorative effects of corn silk extract on Acetaminophen-induced renal toxicity in rats. *Environ Sci Polluti R*. 2021;28:1762–1774. doi:10.1007/s11356-020-10588-4
15. Singh J, Rasane P, Nanda V, Kaur S. Bioactive compounds of corn silk and their role in management of glycaemic response. *J Food Sci Tech*. 2023;60(6):1695–1710. doi:10.1007/s13197-022-05442-z

16. Adewole E, Ojo A, Omoaghe AO. Antidiabetic potential of corn silk extracts, identification and drug properties of bioactive compounds. *Trends Med.* 2018;18(6):1–7.
17. Wang GQ, Xu T, Bu XM, Liu BY. Anti-inflammation effects of corn silk in a rat model of carrageenin-induced pleurisy. *Inflammation.* 2012;35:822–827. doi:10.1007/s10753-011-9382-9
18. Wang X, Yuan L, Bao Z. Screening of uric acid-lowering active components of corn silk polysaccharide and its targeted improvement on renal excretory dysfunction in hyperuricemia mice. *J Funct Foods.* 2021;86:104698. doi:10.1016/j.jff.2021.104698
19. Zou GJ, Huang WB, Sun XY, Tang GH, Ouyang JM. Carboxymethylation of corn silk polysaccharide and its inhibition on adhesion of nanocalcium oxalate crystals to damaged renal epithelial cells. *ACS Biomater Sci Eng.* 2021;7(7):3409–3422. doi:10.1021/acsbiomaterials.1c00176
20. Cheng L, Wang Y, He X, Wei X. Preparation, structural characterization and bioactivities of Se-containing polysaccharide: a review. *Int J Biol Macromol.* 2018;120:82–92. doi:10.1016/j.ijbiomac.2018.07.106
21. Wang R, Chen P, Jia F, Tang J, Ma F, Xu B. Characterization and antioxidant activities of polysaccharides from *Panax japonicus* CA Meyer. *Carbohydr Polym.* 2012;88(4):1402–1406. doi:10.1016/j.carbpol.2012.02.026
22. Lian KX, Zhu XQ, Chen J, Liu G, Gu X-L. Selenylation modification: enhancement of the antioxidant activity of a *Glycyrrhiza uralensis* polysaccharide. *Glycoconjugate J.* 2018;35:243–253. doi:10.1007/s10719-018-9817-8
23. Su Y, Li L. Structural characterization and antioxidant activity of polysaccharide from four auriculariales. *Carbohydr Polym.* 2020;229:115407. doi:10.1016/j.carbpol.2019.115407
24. Wang Y, Jia J, Ren X, Li B, Zhang Q. Extraction, preliminary characterization and in vitro antioxidant activity of polysaccharides from *Oudemansiella radicata* mushroom. *Int J Biol Macromol.* 2018;120:1760–1769. doi:10.1016/j.ijbiomac.2018.09.209
25. Li R, Qin X, Liu S, et al. [HNMP]HSO₄ catalyzed synthesis of selenized polysaccharide and its immunomodulatory effect on RAW264.7 cells via MAPKs pathway. *Inter J Bio Macromol.* 2020;160:1066–1077. doi:10.1016/j.ijbiomac.2020.05.261
26. Zhu S, Sun Y, Jia Y, Zhang W. Acid site-regulated solid acids for polysaccharide Se-functionalization: structural explanations for high reactivity. *Carbohydr Polym.* 2021;251:117028. doi:10.1016/j.carbpol.2020.117028
27. Zhu S, Hu J, Liu S, et al. Synthesis of Se-polysaccharide mediated by selenium oxychloride: structure features and antiproliferative activity. *Carbohydr Polym.* 2020;246:116545. doi:10.1016/j.carbpol.2020.116545
28. Zhao M, Bai J, Bu X. Characterization of selenized polysaccharides from *Ribes nigrum* L. and its inhibitory effects on α -amylase and α -glucosidase. *Carbohydr Polym.* 2021;259:117729. doi:10.1016/j.carbpol.2021.117729
29. Gao Z, Zhang C, Tian C, Ren Z, Song X, Wang X. Characterization, antioxidation, anti-inflammation and renoprotection effects of selenized mycelia polysaccharides from *Oudemansiella radicata*. *Carbohydr Polym.* 2018;181:1224–1234. doi:10.1016/j.carbpol.2017.12.007
30. Corazzari I, Nisticò R, Turci F. Advanced physico-chemical characterization of chitosan by means of TGA coupled on-line with FTIR and GCMS: thermal degradation and water adsorption capacity. *Polym Degrad Stab.* 2015;112:1–9. doi:10.1016/j.polymdegradstab.2014.12.006
31. Hashem AH, Salem SS. Green and ecofriendly biosynthesis of selenium nanoparticles using *Urtica dioica* (stinging nettle) leaf extract: antimicrobial and anticancer activity. *Biotechnol J.* 2022;17(2):2100432. doi:10.1002/biot.202100432
32. Ahmed MK, Moydeen AM, Ismail AM, El-Naggar ME, Menazea AA, El-Newehy MH. Wound dressing properties of functionalized environmentally biopolymer loaded with selenium nanoparticles. *J Molecul Struct.* 2021;1225:129138. doi:10.1016/j.molstruc.2020.129138
33. Bothara SB, Singh S. Thermal studies on natural polysaccharide. *Asian Pac J Trop Biomed.* 2012;2(2):S1031–S1035. doi:10.1016/S2221-1691(12)60356-6
34. Gao P, Bian J, Xu S, Liu C, Sun Y, Zhang G. Structural features, selenization modification, antioxidant and anti-tumor effects of polysaccharides from alfalfa roots. *Int J Boil Macromol.* 2020;149:207–214. doi:10.1016/j.ijbiomac.2020.01.239
35. Wang YF, Hou GH, Li JL, Surhio MM, Ye M. Structure characterization, modification through carboxymethylation and sulfation, and in vitro antioxidant and hypoglycemic activities of a polysaccharide from *Lachnum* sp. *Process Biochem.* 2018;72:177–187. doi:10.1016/j.procbio.2018.06.002
36. Liu D, Xu J, Qian G, et al. Selenizing astragalus polysaccharide attenuates PCV2 replication promotion caused by oxidative stress through autophagy inhibition via PI3K/AKT activation. *Int J Bio Macromol.* 2018;108:350–359. doi:10.1016/j.ijbiomac.2017.12.010
37. Qin T, Ren Z, Huang Y. Selenizing *Herichium erinaceus* polysaccharides induces dendritic cells maturation through MAPK and NF- κ B signaling pathways. *Int J Bio Macromol.* 2017;97:287–298. doi:10.1016/j.ijbiomac.2017.01.039
38. Xu Y, Liu N, Fu X. Structural characteristics, biological, rheological and thermal properties of the polysaccharide and the degraded polysaccharide from raspberry fruits. *Int J Bio Macromol.* 2019;132:109–118. doi:10.1016/j.ijbiomac.2019.03.180
39. Wu C, Zhao M, Bu X, Qing Z, Wang L, Xu Y. Preparation, characterization, antioxidant and antiglycation activities of selenized polysaccharides from blackcurrant. *RSC Adv.* 2020;10(54):32616–32627. doi:10.1039/D0RA06462A
40. Zhu J, Yu C, Han Z, Chen Z, Wei X, Wang Y. Comparative analysis of existence form for selenium and structural characteristics in artificial selenium-enriched and synthetic selenized green tea polysaccharides. *Int J Biol Macromol.* 2020;154:1408–1418. doi:10.1016/j.ijbiomac.2019.11.022
41. Kolsi RBA, Salah HB, Jardak N. Sulphated polysaccharide isolated from *Sargassum vulgare*: characterization and hypolipidemic effects. *Carbohydr Polym.* 2017;170:148–159. doi:10.1016/j.carbpol.2017.04.083
42. Shao C, Zhong J, Liu J, Yang Y, Li M, Yu Y. Preparation, characterization and bioactivities of selenized polysaccharides from *Lonicera caerulea* L. fruits. *Int J Bio Macromol.* 2023;225:484–493. doi:10.1016/j.ijbiomac.2022.11.105
43. Jia Y, Wang Y, Li R, et al. The structural characteristic of acidic-hydrolyzed corn silk polysaccharides and its protection on the H₂O₂-injured intestinal epithelial cells. *Food Chem.* 2021;356:129691. doi:10.1016/j.foodchem.2021.129691
44. Yu J, Ji H, Yang Z, Liu A. Relationship between structural properties and antitumor activity of Astragalus polysaccharides extracted with different temperatures. *Int J Biol Macromol.* 2019;124:469–477. doi:10.1016/j.ijbiomac.2018.11.156
45. Chen W, Zhu X, Ma J, Zhang M, Wu H. Structural elucidation of a novel pectin-polysaccharide from the petal of *Saussurea laniceps* and the mechanism of its anti-HBV activity. *Carbohydr Polym.* 2019;223:115077. doi:10.1016/j.carbpol.2019.115077
46. Cai L, Zou S, Liang D, Luan L. Structural characterization, antioxidant and hepatoprotective activities of polysaccharides from *Sophorae tonkinensis* Radix. *Carbohydr Polym.* 2018;184:354–365. doi:10.1016/j.carbpol.2017.12.083
47. Guo Q, Xu L, Chen Y, et al. Structural characterization of corn silk polysaccharides and its effect in H₂O₂ induced oxidative damage in L6 skeletal muscle cells. *Carbohydr Polym.* 2019;208:161–167.

48. He L, Yan B, Yao C, et al. Oligosaccharides from *Polygonatum Cyrtonema* Hua: structural characterization and treatment of LPS-induced peritonitis in mice. *Carbohydr Polym.* **2021**;255:117392.
49. Li B, Zhang N, Wang DX. Structural analysis and antioxidant activities of neutral polysaccharide isolated from *Epimedium koreanum* Nakai. *Carbohydr Polym.* **2018**;196:246–253. doi:10.1016/j.carbpol.2018.05.037
50. Wang Y, Wei X, Wang F, Xu J, Tang X, Li N. Structural characterization and antioxidant activity of polysaccharide from ginger. *Int J Biol Macromol.* **2018**;111:862–869. doi:10.1016/j.ijbiomac.2018.01.087
51. Farhadi N. Structural elucidation of a water-soluble polysaccharide isolated from *Balangu shirazi* (*Lallemantia royleana*) seeds. *Food Hydrocolloid.* **2017**;72:263–270. doi:10.1016/j.foodhyd.2017.05.028
52. Kokoulin MS, Kuzmich AS, Romanenko LA. Sulfated O-polysaccharide with anticancer activity from the marine bacterium *Poseidonocella sedimentorum* KMM 9023T. *Carbohydr Polym.* **2018**;202:157–163.
53. Wei D, Chen T, Yan M, et al. Synthesis, characterization, antioxidant activity and neuroprotective effects of selenium polysaccharide from *Radix hedysari*. *Carbohydr Polym.* **2015**;125:161–168.
54. Li Y, Yan G, Zhang J, et al. LncRNA HOXA11-AS regulates calcium oxalate crystal-induced renal inflammation via miR-124-3p/MCP-1. *J Cell Molecule Med.* **2020**;24(1):238–249. doi:10.1111/jcmm.14706
55. Próchnicki T, Latz E. Inflammasomes on the crossroads of innate immune recognition and metabolic control. *Cell Metab.* **2017**;26(1):71–93. doi:10.1016/j.cmet.2017.06.018
56. Hwang D, Kang M, Jo MJ, Seo YB, Park NG, Kim GD. Anti-inflammatory activity of β -thymosin peptide derived from pacific oyster (*Crassostrea gigas*) on NO and PGE2 production by down-regulating NF- κ B in LPS-induced RAW264. 7 macrophage cells. *Mar Drugs.* **2019**;17(2):129. doi:10.3390/md17020129
57. Cross RK, Wilson KT. Nitric oxide in inflammatory bowel disease. *Inflamm Bowel Dis.* **2003**;9(3):179–189. doi:10.1097/00054725-200305000-00006
58. Jia Y, Gao X, Xue Z, et al. Characterization, antioxidant activities, and inhibition on α -glucosidase activity of corn silk polysaccharides obtained by different extraction methods. *Int J Biol Macromol.* **2020**;163:1640–1648. doi:10.1016/j.ijbiomac.2020.09.068
59. Khaskheli SG, Zheng W, Sheikh SA. Characterization of *Auricularia auricula* polysaccharides and its antioxidant properties in fresh and pickled product. *Int J Biol Macromol.* **2015**;81:387–395. doi:10.1016/j.ijbiomac.2015.08.020
60. Wang J, Hu S, Nie S, Yu Q, Xie M. Reviews on mechanisms of in vitro antioxidant activity of polysaccharides. *Oxid Med Cell Long.* **2016**;2016:5692852. doi:10.1155/2016/5692852
61. Liu X, Xu S, Ding X, et al. Structural characteristics of *Medicago Sativa* L. Polysaccharides and Se-modified polysaccharides as well as their antioxidant and neuroprotective activities. *Int J Biol Macromol.* **2020**;147:1099–1106. doi:10.1016/j.ijbiomac.2019.10.078
62. Hou R, Li Q, Liu J, Hu Y. Selenylation modification of *Atractylodes macrocephala* polysaccharide and evaluation of antioxidant activity. *Adv Polym Tech.* **2019**;2019:8191385.
63. Li Q, Zhu L, Qi X, et al. Immunostimulatory and antioxidant activities of the selenized polysaccharide from edible *Grifola frondosa*. *Food Sci Nutr.* **2022**;10(4):1289–1298. doi:10.1002/fsn3.2764
64. Li Z, Nie K, Wang Z, Luo D. Quantitative structure activity relationship models for the antioxidant activity of polysaccharides. *PLoS One.* **2016**;11(9):e0163536. doi:10.1371/journal.pone.0163536
65. Wang Z, Zheng Y, Lai Z, et al. Effect of monosaccharide composition and proportion on the bioactivity of polysaccharides: a review. *Int J Biol Macromol.* **2024**;254:127955. doi:10.1016/j.ijbiomac.2023.127955
66. Tsuji H, Wang W, Sunil J, et al. Involvement of renin-angiotensin-aldosterone system in calcium oxalate crystal induced activation of NADPH oxidase and renal cell injury. *World J Urol.* **2016**;34(1):89–95. doi:10.1007/s00345-015-1563-y
67. Song X, Zhang L, Hui X. Selenium-containing protein from selenium-enriched *Spirulina platensis* antagonizes oxygen glucose deprivation-induced neurotoxicity by inhibiting ROS-mediated oxidative damage through regulating MPTP opening. *Pharm Biol.* **2021**;59(1):627–636. doi:10.1080/13880209.2021.1928715
68. Kim SJ, Kim HS, Seo YR. Understanding of ROS-inducing strategy in anticancer therapy. *Oxid Med Cell Longev.* **2019**;2019:5381692. doi:10.1155/2019/5381692
69. Villalpando-Rodriguez GE, Gibson SB. Reactive oxygen species (ROS) regulates different types of cell death by acting as a rheostat. *Oxid Med Cell Longev.* **2021**;2021(1):9912436. doi:10.1155/2021/9912436
70. Zhan Q, Chen Y, Guo Y, Wang Q, Wu H, Zhao L. Effects of selenylation modification on the antioxidative and immunoregulatory activities of polysaccharides from the pulp of *Rose laevigata* Michx fruit. *Int J Biol Macromol.* **2022**;206:242–254. doi:10.1016/j.ijbiomac.2022.02.149
71. Zheng Z, Huang Q, Luo X, Xiao Y, Cai W, Ma H. Effects and mechanisms of ultrasound-and alkali-assisted enzymolysis on production of water-soluble yeast β -glucan. *Bio Technol.* **2019**;273:394–403. doi:10.1016/j.biortech.2018.11.035
72. Qiu J, Zhang H, Wang Z. Ultrasonic degradation of Polysaccharides from *Auricularia auricula* and the antioxidant activity of their degradation products. *Lwt.* **2019**;113:108266. doi:10.1016/j.lwt.2019.108266
73. Xu Y, Zhang X, Yan XH. Characterization, hypolipidemic and antioxidant activities of degraded polysaccharides from *Ganoderma lucidum*. *Int J Biol Macromol.* **2019**;135:706–716. doi:10.1016/j.ijbiomac.2019.05.166
74. Odland B, Dencker L, Tengblad A. Preferential localization of 3H-Pentosanpolysulphate to the urinary tract in rats. *Toxicol Pharmacol.* **1987**;61(3):162–166. doi:10.1111/j.1600-0773.1987.tb01796.x
75. Xia H, Yang C, Zhou B, et al. Pharmacokinetics and excretion study of *Lycium barbarum* polysaccharides in rats by FITC-fluorescence labeling. *Foods.* **2021**;10(11):2851. doi:10.3390/foods10112851
76. Tostes V, Martinusso CA, Werneck CCC, Mourao PS, Cardoso LR. Low-molecular-weight dextran sulfate prevents experimental urolithiasis in rats. *Clin. Chim. Acta.* **2004**;341(1–2):147–155. doi:10.1016/j.cccn.2003.11.015
77. Khan SR, Canales BK, Dominguez-Gutierrez PR, Randall's plaque and calcium oxalate stone formation: role for immunity and inflammation. *Nat Rev Nephrol.* **2021**;17(6):417–433. doi:10.1038/s41581-020-00392-1
78. Liu JH, Ouyang JM. Synergistic inhibition of calcium oxalate crystal formation and synergistic protection of HK-2 cells from crystal damage by sulfated Laminarin polysaccharide and potassium citrate. *Biomater Sci UK.* **2023**;11(10):3524–3546. doi:10.1039/D3BM00087G
79. Hou C, Chen L, Yang L, Ji X. An insight into anti-inflammatory effects of natural polysaccharides. *Int J Biol Macromol.* **2020**;153:248–255. doi:10.1016/j.ijbiomac.2020.02.315

80. Sanchez-Lopez E, Coras R, Torres A, Lane NE, Guma M. Synovial inflammation in osteoarthritis progression. *Nat Rev Rheumatol.* **2022**;18(5):258–275. doi:10.1038/s41584-022-00749-9
81. Sang T, Guo C, Guo D, Wu J, Wang Y, Wang X. Suppression of obesity and inflammation by polysaccharide from sporoderm-broken spore of *Ganoderma lucidum* via gut microbiota regulation. *Carbohydr Polym.* **2021**;256:117594. doi:10.1016/j.carbpol.2020.117594
82. Liu Y, Ye Y, Hu X, Wang J. Structural characterization and anti-inflammatory activity of a polysaccharide from the lignified okra. *Carbohydr Polym.* **2021**;265:118081. doi:10.1016/j.carbpol.2021.118081
83. Lee JH, Lee YK, Choi YR, Park J, Jung SK, Chang YH. The characterization, selenylation and anti-inflammatory activity of pectic polysaccharides extracted from *Ulmus pumila* L. *Int J Biol Macromol.* **2018**;111:311–318. doi:10.1016/j.ijbiomac.2018.01.005
84. Hamid M, Liu D, Abdulrahim Y. Inactivation of kupffer cells by selenizing astragalus polysaccharides prevents CCI 4-induced hepatocellular necrosis in the male Wistar rat. *Biol Trace Elem Res.* **2017**;179:226–236. doi:10.1007/s12011-017-0970-x
85. Ma J, Qiao Z, Xiang X. Optimisation of extraction procedure for black fungus polysaccharides and effect of the polysaccharides on blood lipid and myocardium antioxidant enzymes activities. *Carbohydr Polym.* **2011**;84:1061–1068. doi:10.1016/j.carbpol.2010.12.068
86. Wang J, Yang X, Bao A, et al. Microwave-assisted synthesis, structure and anti-tumor activity of selenized *Artemisia sphaerocephala* polysaccharide. *Int J Biol Macromol.* **2017**;95:1108–1118. doi:10.1016/j.ijbiomac.2016.10.101
87. Zhao B, Zhang J, Yao J, Song S, Yin Z, Gao Q. Selenylation modification can enhance antioxidant activity of *Potentilla anserina* L. polysaccharide. *Int J Biol Macromol.* **2013**;58:320–328. doi:10.1016/j.ijbiomac.2013.04.059
88. Wang Z, Zheng Y, Hu Y, et al. Improvement of antibacterial activity of polysaccharides via chemical modification: a review. *Int J Biol Macromol.* **2024**;132:163. doi:10.1016/j.ijbiomac.2024.132163
89. Liu Y, Sun Y, Kang J, et al. Role of ROS-induced NLRP3 inflammasome activation in the formation of calcium oxalate nephrolithiasis. *Front Immunol.* **2022**;13:818625. doi:10.3389/fimmu.2022.818625
90. Wang Z, Wang L, Yu X, et al. Effect of polysaccharide addition on food physical properties: a review. *Food Chem.* **2023**;2023:137099.
91. He Y, Zhang C, Zheng Y, et al. Effects of blackberry polysaccharide on the quality improvement of boiled chicken breast. *Food Chem X.* **2023**;18:100623. PMID: 36935905; PMCID: PMC10020652. doi:10.1016/j.fochx.2023.100623

Publish your work in this journal

The Journal of Inflammation Research is an international, peer-reviewed open-access journal that welcomes laboratory and clinical findings on the molecular basis, cell biology and pharmacology of inflammation including original research, reviews, symposium reports, hypothesis formation and commentaries on: acute/chronic inflammation; mediators of inflammation; cellular processes; molecular mechanisms; pharmacology and novel anti-inflammatory drugs; clinical conditions involving inflammation. The manuscript management system is completely online and includes a very quick and fair peer-review system. Visit <http://www.dovepress.com/testimonials.php> to read real quotes from published authors.

Submit your manuscript here: <https://www.dovepress.com/journal-of-inflammation-research-journal>